SEL-63-130

The Calculation of Electron Density Profiles from Topside Ionograms Using a Digital Computer

by
J. O. Thomas and D. Westover

August 1963

Technical Report No. 5

Prepared under
National Aeronautics and Space Administration
Grant NsG 30-60

RADIOSCIENCE LABORATORY
STANFORD ELECTRONICS LABORATORIES
STANFORD UNIVERSITY • STANFORD, CALIFORNIA

RC
#3

SEL-63-130

THE CALCULATION OF ELECTRON DENSITY PROFILES FROM TOPSIDE IONOGRAMS USING A DIGITAL COMPUTER

by

J. O. Thomas and D. Westover

August 1963

Technical Report No. 5

Prepared under
National Aeronautics and Space Administration
Grant NsG 30-60

Radioscience Laboratory
Stanford Electronics Laboratories
Stanford University Stanford, California

ACKNOWLEDGEMENTS

The authors wish to acknowledge gratefully the courtesy of scientists of the Canadian Defence Research Telecommunications Establishment, Ottawa, Canada, particularly Dr. J.H. Chapman and Dr. G.L. Nelms who made a number of topside ionograms available to the authors in the early stages of development of this work.

They wish also to thank the Canadian Defence Research Telecommunications Establishment and the National Aeronautics and Space Administration for permission to monitor signals from the Alouette satellite at Stanford. The telemetry receiving station at Stanford has been operated by Messrs. S. Hall, D. Annett, and K. Byram, and the data were prepared for analysis by D. Annett and A.Y. Sader. It is a pleasure to acknowledge the efforts of all of these contributors to the program of work described in this report.

The interest of Professors O.G. Villard, Jr. and O.K. Garriott of the Radioscience Laboratory is gratefully acknowledged.

The work was financed by a grant, NsG 30-60 from the National Aeronautics and Space Administration.

Contents

FIGURE AND TABLE CAPTIONS

TABLES

ILLUSTRATIONS

Abstract

13547

An ionosonde situated in a vehicle immersed in the plasma above the peak of the F2 layer of the ionosphere, measures, as a function of frequency, f, the virtual depth, h', below the vehicle, at which radio waves are reflected from the topside of the ionosphere. In this paper, a digital computer program for converting the observed, topside $h'(f)$ curves, into electron density profiles using the method presented by Thomas, Long, and Westover, (1963), is described. The program, although designed specifically for the reduction of topside sounder records from the Canadian "Alouette" satellite may also be used for the analysis of records from ground-based ionosondes.

THE CALCULATION OF ELECTRON DENSITY PROFILES FROM TOPSIDE IONOGRAMS USING A DIGITAL COMPUTER

J.O. Thomas and D. Westover
Radioscience Laboratory
Stanford University

I. Introduction

The Canadian topside sounder "Alouette" was launched into orbit around the earth on September 29, 1962 [C.D.R.T.E. (1962), Warren (1962), Thomas (1963)]. Telemetered signals from this satellite have been received at Stanford University since December 4, 1962 so that ionograms giving the variation of the virtual depth of reflection of radio waves reflected by the topside of the ionosphere as a function of their frequency, f, ($h'(f)$ curves) have been available on a routine basis since that date. Details concerning the construction, operation and orbit characteristics of the satellite can be found in the references quoted above. The program of observation and a description of the ionograms recorded at Stanford, together with a bibliography of papers published in the topside sounder field to date (August 1963) are presented in another Technical Report in the Stanford Electronics Laboratories Series (Thomas and Sader 1963). These topside ionograms contain information about the distribution of electron density with height in the lower exosphere, a detailed knowledge of which is extremely important for the physics of the ionosphere. The derivation of the electron density information from the ionogram is, however, a complicated procedure and is best carried out on a digital computer. This report presents information concerning such a program which has been arranged for the Stanford IBM 7090 digital computer using the method suggested by Thomas, Long, and Westover (1963). The development and test-

ing of the program together with details concerning the operational procedures to be employed for converting an ionogram into an electron-density profile (N(h) curve) are described in detail below.

II. Description of the calculation

The problem of converting virtual height-frequency records, ($h'(f)$ curves) produced by ground-based ionosondes to electron density-height profiles (N(h) curves) has been the subject of a large number of papers in ionospheric physics and has been solved in a number of ways. The corresponding reduction of the records likely to be obtained by an ionosonde situated in a vehicle, such as a rocket or satellite, immersed in the plasma above the peak of the F2 layer, though basically similar in nature, involves, however, some interesting features not encountered in the analysis of ground-based data. These differences have been outlined in a recent paper by Thomas, Long and Westover (1963) in which a method for converting the topside sounder observations into electron density profiles was presented. This method is described briefly below and forms the basis of the Stanford IBM 7090 digital computer program for the calculation of electron density profiles from topside ionograms.

The quantities recorded in topside sounder experiments are the virtual depths of reflection of radio pulses incident normally on the upper F region as a function of frequency, f, and these will be referred to as the observed $h'(f)$ data. The N(h) profile corresponding to the observed $h'(f)$ curve is obtained using the assumption that the complete real height curve can be represented by a polynomial in $(f_N - f_o)$ where f_N is the plasma frequency and f_o is the value of f_N at the vehicle. This polynomial is the one of lowest degree in $(f_N - f_o)$ which can produce the observed virtual depths of reflection so that the method produces the smoothest possible real-height curve which can explain the experimental observations. It is assumed

that the plasma frequency, f_o, at the vehicle is known. This quantity may be readily derived accurately from measurements of the frequencies at which plasma spikes are observed [Lockwood (1962), Thomas & Sader (1963)]. These spikes together with the cyclotron spikes may also be used to calculate the magnetic dip angle I, and the gyro frequency for electrons, at the location of the satellite which are required in the calculation. In practice, however, sufficient accuracy in the derived N(h) profiles may be obtained by utilizing extrapolations of the magnetic field as measured at the ground.

The basic procedures of the polynomial method can be used in two distinct ways. In the first method, which we shall refer to as the "single polynomial method," the complete N(h) profile is approximated to by a single polynomial, so that $h'(f)$ data covering the whole of the relevant plasma frequency range is utilized. This method for the case of monotonic profiles is more accurate than a lamination method with the same number of readings of h' (Titheridge 1961). It has the distinct advantage that in practice only a few observations of h' are necessary. The second method, which we shall refer to as the "overlapping polynomial" method can be made, in practice, as accurate as is desirable and is suitable for the analysis of $h'(f)$ curves containing "cusps." In this case, rather more readings will be required from the $h'(f)$ curve than would be necessary for the single polynomial method, but where the increased accuracy available by the overlapping polynomial method is required, then it is the best method to use and is in general the one which is applied for the analysis of $h'(f)$ data obtained at Stanford. This report is concerned only with the single polynomial method. A discussion of the details relative to the overlapping polynomial method is presented elsewhere, (Thomas and Westover 1963).

II.1. Special Problems in Topside Sounder $h'(f)$ Analysis

It is assumed throughout that the ionosphere is uniform and that there are no gradients of ionization in any direction other than the vertical. The mathematical problem involved in deducing an N(h) profile from the observed topside $h'(f)$ curve differs from the corresponding problem for the case of a ground-based ionosonde in several important respects which are outlined below.

First, the transmitter is immersed in the ionosphere, so that all virtual depths are measured not from a region where the plasma frequency is zero, but from a region where the plasma frequency has some finite, non-zero value, which we shall call f_o. For this reason, it is not possible without loss of accuracy to apply directly any of the existing $h'(f)$ to N(h) reduction techniques developed for the analysis of ground-based ionograms, unless $f_o \approx o$, since the expression which is used as the starting basis for these methods for the Ordinary ray, for example, takes the form

$$h' = \int_o^{f_i} \mu_o'(f_i, f_N) \frac{dh}{df_N} df_N \qquad (1)$$

where $\mu_o'(f_i, f_N)$ is the Ordinary ray group refractive index at the wave frequency f_i and plasma frequency f_N. In the case in which the transmitter is immersed in the medium, the lower limit of this integral is f_o, and not zero.

Secondly, the gradient dh/df_N at the vehicle from which the $h'(f)$ observations are being made is finite, whereas it is usually assumed (Titheridge, 1961) that it is zero at the bottom of the ionosphere (where N=o) in the analysis of ground-based ionograms.

The calculation described in the next section takes into account these specific topside ionogram problems and may be used for the reduction to N(h) profiles of continuous topside $h'(f)$ curves similar to those obtained by the Canadian topside sounder Alouette or of "spot-frequency" ionograms of the kind to be obtained by the proposed American topside sounder S48 (Knecht et al 1962). The method may also be used for the reduction of ground-based ionograms to electron density profiles.

II.2. Method of Analysis

Throughout this section the following nomenclature is used:

f_o	=	plasma frequency at the vehicle
h	=	real height measured from the ground
h_o	=	height of the vehicle measured from the ground
h_i'	=	virtual depth of reflection, measured positively downward from the vehicle, of a radio wave of frequency f_i,
Δh_i	=	real depth, measured positively downward from the vehicle, of the level at which the plasma frequency is f_i.

Only the method for the conversion of the Ordinary ray $h'(f)$ trace into an N(h) profile is considered in detail; the Extraordinary ray $h'(f)$ trace may be treated by a basically similar procedure which is indicated. It is assumed that the real depths, Δh_i, and the virtual depths, h_i', are measured from the level, h_o, at which the plasma frequency $f_N=f_o$, so that $h=h_o$ at $f_N=f_o$. It is also assumed that where $f_N=f_o$, dh/df_N is finite, but non-zero. The real-height curve may then be given as a function of plasma frequency, f_N, by the equations which follow:

$$h_o = \alpha_o' + \alpha_1' (f_o-f_o) + \alpha_2' (f_o-f_o)^2 + ...\alpha_n' (f_o-f_o)^n = \alpha_o'$$

$$h_1 = \alpha_o' + \alpha_1' (f_1-f_o) + \alpha_2' (f_1-f_o)^2 + ...\alpha_n' (f_1-f_o)^n$$

$$\vdots$$

$$h_n = \alpha_o' + \alpha_1' (f_n-f_o) + \alpha_2' (f_n-f_o)^2 + ...\alpha_n' (f_n-f_o)^n$$

i.e.

$$h = \sum_{j=o}^{n} \alpha_j' (f_N-f_o)^j; \quad h_o = \alpha_o' = \text{constant} \qquad (2)$$

Writing $\alpha_n = -\alpha_n'$ throughout, the real depths of reflection measured from the vehicle may then be written

$$h_o - h_1 = \Delta h_1 = \alpha_1(f_1-f_o) + \alpha_2(f_1-f_o)^2 + \ldots\alpha_n(f_1-f_o)^n$$

$$h_o - h_2 = \Delta h_2 = \alpha_1(f_2-f_o) + \alpha_2(f_2-f_o)^2 + \ldots\alpha_n(f_2-f_o)^n$$

$$\vdots$$

$$h_o - h_n = \Delta h_n = \alpha_1(f_n-f_o) + \alpha_2(f_n-f_o)^2 + \ldots\alpha_n(f_n-f_o)^n$$

i.e.

$$\Delta h = \sum_{j=1}^{n} \alpha_j (f_N-f_o)^j \qquad (2a)$$

These equations may be written in matrix notation as

$$\underline{\Delta h} = \underline{A}\ \underline{\alpha} \qquad (3)$$

where $\underline{A}$ is an n by n matrix with the typical element

$$a_{ij} = (f_i-f_o)^j$$

It should be noted that (2) differs from the corresponding expression given by Titheridge (1961) in that Δh is given by a polynomial in (f_N-f_o) rather than in f_N, and that (2)

allows for a finite gradient, dh/df_N, at the vehicle (or at the base of the ionosphere in the case of ground-based ionograms).

The virtual depth h_i' at the frequency f_i is given by

$$h_i' = \int_o^{\Delta h_i} \mu_o'(f_i, f_N)\, d(\Delta h) \tag{4}$$

Substituting the value of $d(\Delta h)$ obtained from equation (2a) gives

$$h_i' = \sum_{j=1}^{n} b_{ij}\alpha_j \; ; \; h_o' = o \tag{5}$$

where

$$b_{ij} = j\int_{f_o}^{f_i} \mu_o'(f_i, f_N)(f_N - f_o)^{j-1} df_N \tag{6}$$

As before, the set of equations represented by (5) can be written in matrix notation as

$$\underline{h}' = \underline{B}\,\underline{\alpha} \tag{7}$$

where $\underline{B}$ is an n by n matrix with typical elements given by (6).

Relations (3) and (7) may now be combined to give

$$\underline{\Delta h} = (\underline{AB}^{-1})\,\underline{h}' = \underline{Ch}' \tag{8}$$

$\underline{C} = (\underline{AB}^{-1})$ is now an n by n matrix which depends only on the frequencies, f_o, f_i, and on the Ordinary ray group refractive index, μ_o'.

For the case of the Extraordinary ray trace, (the $h'_x(f)$ curve) the procedure is basically the same, but (1) becomes

$$h'_x = \int_{f_o}^{f'_i} \mu'_x(f'_i, f_N) \frac{dh}{df_N} df_N \tag{9}$$

Where the frequencies f_{xi} and corresponding h'_{xi} are measured on the Extraordinary ray trace and f_o and f'_i are the plasma frequencies corresponding to the frequencies f_{xv} and f_{xi} given by

$$\begin{aligned} f_{xv}^2 &= f_o^2 + f_{xv}\, f_{Hv} \quad (f_{xv} > f_{Hv}) \\ f_{xi}^2 &= f_i'^2 + f_{xi}\, f_{Hi} \quad (f_{xi} > f_{Hi}) \end{aligned} \tag{10}$$

in which f_{xv} is the frequency (measured on the Extraordinary trace) at which $h'_x = o$, f_{Hv} is the value of the gyro-frequency for electrons at the vehicle and f_{Hi} that at the real height of reflection of the frequency f_{xi}. Equation (6) then becomes

$$b_{ij} = j \int_{f_o}^{f'_i} \mu'_x(f'_i, f_N)(f_N - f_o)^{j-1} df_N \tag{11}$$

and the equation corresponding to (8) is

$$\underline{\Delta h} = \underline{C_x h'_x} \tag{12}$$

The calculation of the Ordinary and Extraordinary ray refractive indices μ'_o and μ'_x are described in Section III below.

An alternative form of the solution is presented in Appendix I.

III. The calculation of the group refractive index for the Ordinary and Extraordinary rays

For the calculation of the group refractive index μ_o' for the Ordinary ray and μ_x' for the Extraordinary ray, the mathematical formulations of the Appleton-Hartree equations as presented by Becker (1960) are used. The relevant equations are reproduced below. The expressions for μ_x' when $f < f_H$ are also included, (Becker (1963)).

The Appleton-Hartree formula for the refractive indices of an ionized gas may be written

$$n_{o,x}^2 = 1 - \frac{2\, f_o^2/f^2}{2 - \frac{f_T^2/f^2}{1-f_o^2/f^2} \mp \sqrt{\left[\frac{f_T^2/f^2}{1-f_o^2/f^2}\right]^2 + 4\frac{f_L^2}{f^2}}} \qquad (13)$$

in which the suffixes o and x refer to the Ordinary and Extraordinary ray refractive indices. The upper sign in the square root term holds for the Ordinary and the lower for the Extraordinary wave component. Energy losses by electron collisions are neglected. In (13) the symbols used are as follows.

f_o = plasma frequency $= \sqrt{\frac{Ne^2}{\pi m}}$;

N = electron density per cm^3;

e = charge of an electron;

m = mass of an electron;

π = 3.14 159 ... ;

f_H = gyro frequency = $\frac{eH}{2\pi mc}$;

H = total intensity of the earth's magnetic field;

I = angle of inclination of the earth's magnetic field;

$f_L = f_H \sin I$;

$f_T = f_H \cos I$;

f = frequency of observation

The Ordinary and Extraordinary group refractive indices μ_o' and μ_x' are defined by

$$\mu'_{o,x} = \frac{c}{U_{o,x}} = \frac{d}{df}(fn_{o,x}) \qquad (14)$$

where

c = free space velocity of light and

U = Group velocity defined for the o and x rays by the appropriate suffixes.

We may write (14) as

$$\mu'_{o,x} = \frac{c}{U_{o,x}} = \frac{1}{n_{o,x}}\left(1 + \frac{2f_o^2}{N_{o,x}^2} \cdot \frac{dN_{o,x}}{df^2}\right), \qquad (15)$$

where

$$N_{o,x} = 2 - \frac{f_T^2/f^2}{1 - f_o^2/f^2} \pm \sqrt{\left[\frac{f_T^2/f^2}{1 - f_o^2/f^2}\right]^2 + 4\frac{f_L^2}{f^2}},$$

and

$$2f_o^2 \frac{dN_{o,x}}{df^2} = \frac{\frac{4f_o^2 f_L^2}{f^4} \cdot \frac{1+f_o^2/f^2}{1-f_o^2/f^2}}{\pm\sqrt{\left[\frac{f_T^2/f^2}{1-f_o^2/f^2}\right]^2 + 4\frac{f_L^2}{f^2}}} - \frac{2f_o^2/f^2}{1-f_o^2/f^2}\left[N_{o,x}^{-2}\right].$$

A Taylor approximation to the group refractive indices may, if necessary, be used for small plasma frequencies:

$$f_o \Big/ \lim_{f \to o} \frac{c}{U_{o,x}} = \lim \left(1 + \frac{f_o^2}{f^2} A_{o,x} + \cdots\right) = 1. \qquad (16)$$

The coefficients $A_{o,x}$ are derived from equation (15) and are:

$$A_{o,x} = \frac{4}{N_{o,x}^2} \left(1 \pm \frac{f_L^2/f^2}{\sqrt{\frac{f_T^4}{f^4} + 4\frac{f_L^2}{f^2}}}\right) - \frac{1}{N_{o,x}} . \qquad (17)$$

III.1. Numerical calculation of μ_o' and μ_x'

It is useful to define (Shinn 1954, Becker 1959)

O-ray

$$\mu_o' \, t = G_o$$

where

$$t^2 = 1 - f_o^2/f^2$$

X-ray

$$\mu_x' \, t_R = G_R$$

where

$$t_R^2 = 1 - f_o^2/f_R^2$$

in which

$$f_R^2 = f_x^2 - f_x f_H \quad f_x > f_H$$

$$f_R^2 = f_x^2 + f_x f_H \quad f_x < f_H$$

where f_x is the Extraordinary frequency of observation.

The Ordinary ray refractive index may be computed from:

$$\left(\frac{n_o}{t_R}\right)^2 = \frac{1+\dfrac{2\tan^2 I}{1+\sqrt{1+\gamma\, t_R^4}}}{1+t_R^2\,\dfrac{2\tan^2 I}{1+\sqrt{1+\gamma t_R^4}}} \quad ; \tag{18}$$

where

$$\gamma = \frac{4\,\tan^2 I}{y_R^2\,\cos^2 I} \quad .$$

thus

$$G_o = \frac{t_R}{n_o}\left\{1+\frac{x_R \tan^2 I}{M^2}\left[\frac{(1+x_R)}{\sqrt{1+\gamma t_R^4}} - \frac{2}{1+\sqrt{1+\gamma t_R^4}}\right]\right\} \tag{19}$$

where

$$M = 1+t_R^2 \cdot \frac{2\tan^2 I}{1+\sqrt{1+\gamma t_R^4}} \quad ; \qquad x_R = 1 - t_R^2 \quad .$$

We may write

$$A_o = \frac{1}{2M_1}\left[\frac{2}{M_1}\left(1+\frac{\tan^2 I}{1+\gamma}\right) - 1\right] \tag{20}$$

where

$$M_1 = 1 + \frac{2\tan^2 I}{1+\sqrt{1+\gamma}}$$

The limiting cases are:

$$\lim_{t_R \to o} \frac{n_o}{t_R} = \frac{1}{\cos I} \; ; \quad \lim_{t_R \to 1} G_o = \lim_{x_R \to o}(1+x_R A_o + .) = 1 \qquad (21)$$

The Extraordinary ray refractive index may be computed from

$$n_x^2 = \pm\, y\xi \, \frac{1 - \dfrac{\beta}{1+\sqrt{1+\alpha\xi}}}{1 \mp y + \Delta \mp \dfrac{\beta y \xi}{1+\sqrt{1+\alpha\xi}}} \; . \qquad (22)$$

Where

$$\alpha = \frac{4\sin^2 I}{(1+\sin^2 I)^2} \; ; \qquad \beta = \frac{2\sin^2 I}{1+\sin^2 I} \; ;$$

$$\xi = 2\Delta + \Delta^2 \; ; \qquad \Delta = t_R^2 \, \frac{1 \mp y}{\pm y} \; ;$$

$$y_R = \frac{f_H}{f_R} \; ; \qquad \frac{1 \mp y}{y} = \frac{1}{2y_R}\left(\sqrt{4+y_R^2} \mp y_R\right) \; ;$$

$$y = \frac{1}{2}\, y_R\left(\sqrt{4+y_R^2} \mp y_R\right).$$

$$G_R = \frac{c}{U_x}\, t_R = \frac{t_R}{n_x}\left[1 + \frac{x}{N^2}\left\{1 + \frac{\beta}{2}\left[\frac{2\xi}{1+\sqrt{1+\alpha\xi}} - \frac{(1+\xi)(1+x)}{\sqrt{1+\alpha\xi}}\right]\right\}\right] \qquad (23)$$

where

$$N = 1 \mp y + \Delta \mp \beta \, \frac{y\xi}{1+\sqrt{1+\alpha\xi}} \; ; \qquad x = x_R(1 \mp y) \; ;$$

$$A_{xR} = (1\mp y)\left[\frac{4}{N_1^2}\left(1-\frac{\tan^2 I}{\sqrt{1+\gamma}}\right) - \frac{1}{N_1}\right] \qquad (24)$$

where

$$\gamma = \frac{4\tan^2 I}{y^2\cos^2 I} \; ; \qquad N_1 = 2-y^2\cos^2 I\left(1+\sqrt{1+\gamma}\right) \; ;$$

$$A_{xR} = A_x(1\mp y) \; .$$

Again the limiting cases are

$$\lim_{t_R \to o} \frac{n_x^2}{t_R^2} = \frac{2}{1+\sin^2 I} \; ; \quad \lim_{t_R \to 1} G_R = \lim_{x_R \to o} \left(1+x_R A_{xR}^{+}.\right)=1 \qquad (25)$$

For purely longitudinal propagation, e.g. $f_H=f_L$, $f_T=o$ the previous formulae reduce to:

$$n_{xL} = t_R \; ; \qquad (26)$$

$$G_{RL} = 1+x_R \cdot \frac{y}{2(1-y)} \; ; \qquad (27)$$

Curves of both the Ordinary and Extraordinary group refractive indices, for several values of I and f_o are reproduced and discussed in Appendix III.

III.2. Application of the Method

A general consideration of the accuracy of the polynomial method of analysis applied to normal ionograms has been given by Titheridge (1961). The same restrictions apply to its use for topside ionograms, in that if the polynomial is of too high an order then an "oscillating" N(h) curve is obtained. Too low an order gives insufficient values for a curve to be well defined. In general, a polynomial of degree 4, 5, 6, 7 or 8 has been found to be most satisfactory and most of the tests devised to check the method have been applied using a fifth-degree polynomial. The method may be applied in two ways:

(i) The matrix $\underline{C}$ may be computed once and for all for any given set of the observing frequencies, f_i, for a given set of values of f_o, and for any given magnetic conditions. These matrices may be tabulated and used as described by Long and Thomas (1963) who have published tables of Titheridge coefficients for the reduction of ground-based ionograms. Coefficients calculated by the method of Section II.2. would be useful for spot frequency observations of the topside of the ionosphere and for the reduction of ionograms corresponding to continuous, cusp-free topside $h'(f)$ curves.

In Table I, the matrix $\underline{C}$ connecting the real depths and the Ordinary Ray virtual depths at six frequencies at the magnetic equator, is presented. These coefficients were computed for f_o = 1 Mc/s and for a set of frequencies, f_i, corresponding to 2, 3, 4, 5, and 6 Mc/s. In order to compute the real depth at, say, a frequency of 5 Mc/s, it is simply necessary to multiply the elements in the fourth row of Table I by the corresponding virtual depths at each frequency 2, 3,....6 Mc/s and to form the sum.

TABLE I.					
f(Mc/s)	Matrix C				
2	0.81237	-0.42971	0.27360	-0.10114	0.01608
3	0.46142	0.24168	0.05278	-0.02551	0.00450
4	0.28116	0.17605	0.38741	-0.04977	0.00703
5	0.23428	0.03256	0.35593	0.22375	-0.00233
6	0.15521	0.13330	0.05396	0.32906	0.19538

Table I. The matrix C connecting the real depths and the Ordinary ray virtual depths at six frequencies at the magnetic equator.

For the reduction of large numbers of ionograms, however, it is best to compute the matrix $\underline{C}$ and to carry out the entire calculation in a digital computer. Examples of profiles computed from ionograms in this way are presented in a later section.

Although the single polynomial method particularly as applied to topside ionograms is likely to be sufficiently accurate for most purposes, greater accuracy may be achieved (at only a relatively small cost in terms of extra data points required) by the method referred to in (ii) below.

(ii) If the topside ionogram shows cusps, the analysis may be applied by fitting a series of polynomials, in overlapping small frequency ranges, to the observations in the manner described by Titheridge (1961) in his "modified" polynomial method. The procedure is described in a separate publication in this series of reports (Thomas and Westover 1963). These cusps may arise because the $N(h)$ profile is not smooth, but contains ledges or distinct changes of slope, or, under certain circumstances, at night, even with a smooth exponential type layer, when the plasma frequency at the vehicle approaches the gyro-frequency for electrons (see Section V.2).

IV. Tests of the method - the accuracy of the calculations

In order to check the method and its accuracy, an $h'(f)$ curve may be calculated for a given $N(h)$ profile of the kind likely to be observed in the upper F region. The calculated $h'(f)$ points may then be used as the starting data and an $N(h)$ profile derived by the method of Section II.2. This calculated profile may then be compared with the original assumed model. The details of the reduction are described below.

IV.1. Model calculations

Several models for the $N(h)$ distribution were assumed. For an exponential model, we may write

$$N = N_o e^{\Delta h / H} \tag{28}$$

where N_o is the value of N at the level of the vehicle, H is the scale height and $\Delta h = h_o - h$ is, as before, the real depth of reflection of the radio wave, so that Δh is the vertical distance measured positively downward from the level at which $f_N = f_o$. For the case of no magnetic field, the corresponding $h'(f)$ curve is of the form (Budden 1961)

$$h' = 2H \operatorname{sech}^{-1} \frac{f_o}{f} \tag{29}$$

A series of virtual height curves were calculated for a number of values of H, and f_o, corresponding to possible ionospheric models of the kind which might be encountered in practice. These $h'(f)$ curves were reduced to $N(h)$ curves using "topside" coefficients calculated by the method of Section II.2 for the no-magnetic field case. An example is given in Figure 1 in which the continuous line is the original $h(f_N)$ curve, computed from (28) with $f_o = 1.0$ Mc/s. The corresponding top-

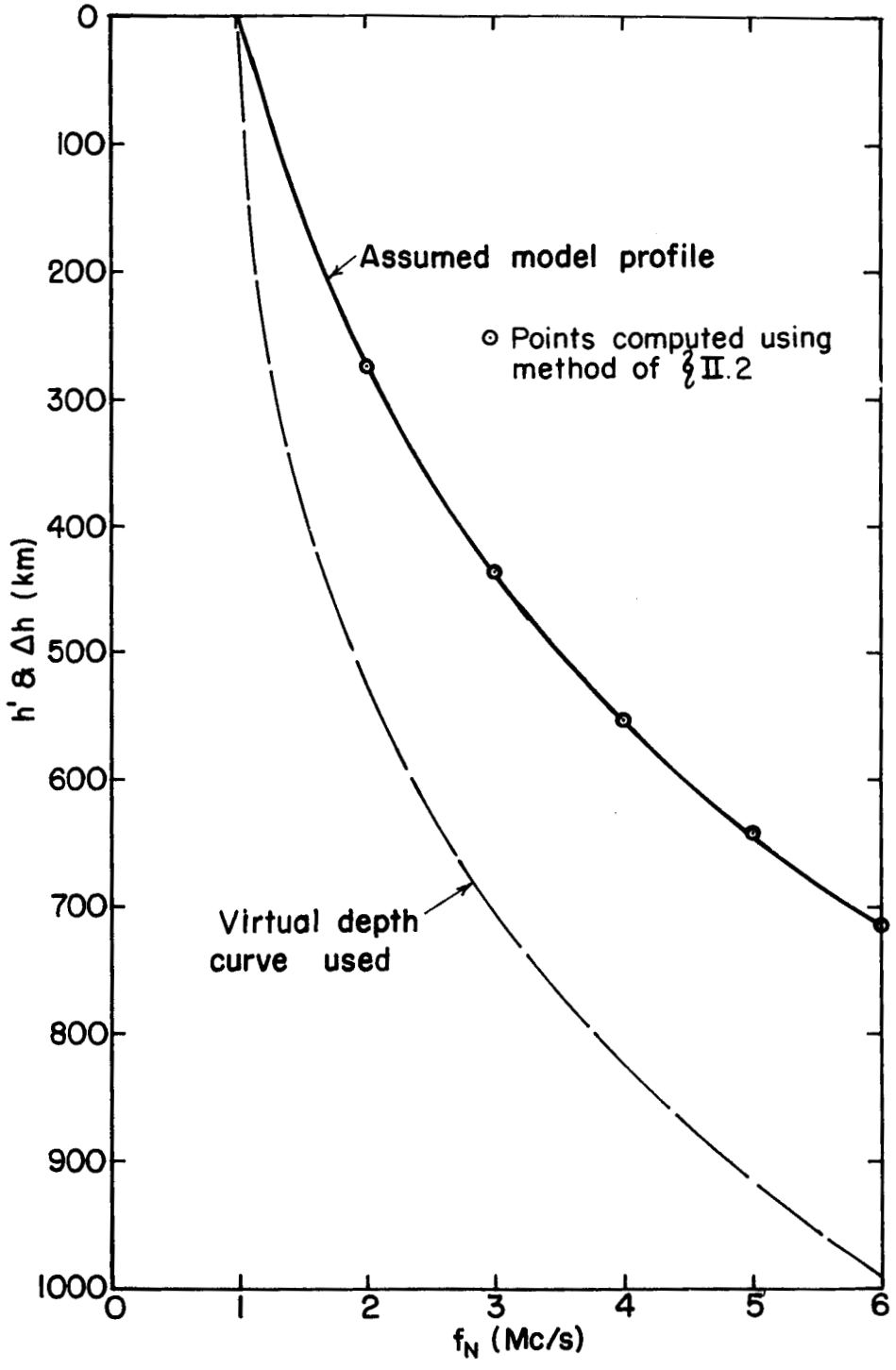

Figure 1: Test of the method of II.2, (exponential model). The upper, continuous line represents the assumed topside electron density model. The lower, broken curve is the corresponding Ordinary ray h'(f) curve calculated for the no-field case. The circles represent the points computed by the technique described in the paper. It will be seen that the original profile can be recovered accurately.

side Ordinary ray h'(f) curve computed from (29) is shown as the lower curve in Figure 1 and the circles show the real depths obtained using the "topside" coefficients derived by the method of Section II.2. It is clear that the $h(f_N)$ curve obtained using these coefficients agrees closely with the original, indicating that the method works to a sufficiently high degree of accuracy.

In these calculations, it was assumed that f_o was known and its value determined which matrices, calculated for different values of f_o, were used in the reduction. If f_o is not in fact known, it may be determined by analyzing the Ordinary and Extraordinary ray h'(f) curves using sets of coefficients corresponding to several values of f_o. The value of f_o which leads to the two resulting N(h) curves being most nearly the same will be the plasma frequency at the vehicle.

Further examples are given below of the way in which an assumed profile may be recovered from the derived h'(f) curve calculated for a number of model ionospheres.

For a parabolic real-depth model, the model itself is represented by:

$$\Delta h = y_m \left(1-\sqrt{1-(f/f_c)^2}\right) \qquad (30)$$

and the corresponding expression for the no-field Ordinary ray virtual depth curve at the magnetic equator is:

$$h' = y_m\left(\frac{f}{f_c}\right) \tanh^{-1}\left(\frac{f}{f_c}\right) \qquad (31)$$

Where:

y_m = semi-thickness of the layer

f_c = critical frequency of the layer

Figure 2 shows the theoretical h' and Δh curves for such a model, with y_m = 100 kilometers, f_c = 6.5 Mc/s. The plasma frequency at the satellite is assumed to be 1 Mc/s. The circled points on the figure represent the values of Δh obtained using values of h' from the calculated h' curve and using the method of section II.2 to reduce them to Δh values.

Figure 3 illustrates the results of the method of section II.2 as applied to a square law model of the form

$$\Delta h = cf^2 \tag{32}$$

$$h' = 2cf^2 \tag{33}$$

where c is an arbitrary constant, in this case chosen to be 10. The plasma frequency at the satellite is assumed to be 0 Mc/s.

Calculations for both Ordinary and Extraordinary rays were also carried out allowing for the effect of the earth's magnetic field. Figure 4 shows the $h'_o(f)$ and $h'_x(f)$ curves corresponding to a Chapman layer computed by Doupnik (1963). The expression used for the Chapman layer is:

$$\frac{f_N^2}{f_c^2} = \exp \frac{1}{2}\left[1 - \frac{(h-h_{max})}{H} - \exp \frac{(h-h_{max})}{H}\right] \tag{34}$$

Where:

f_c = critical frequency of the layer

h_{max} = height above ground corresponding to $f_{N(max)}$

H = scale height of the layer

The h(f) points derived by the 7090 program described in Appendix IV, using these h'(f) curves as data, are shown in

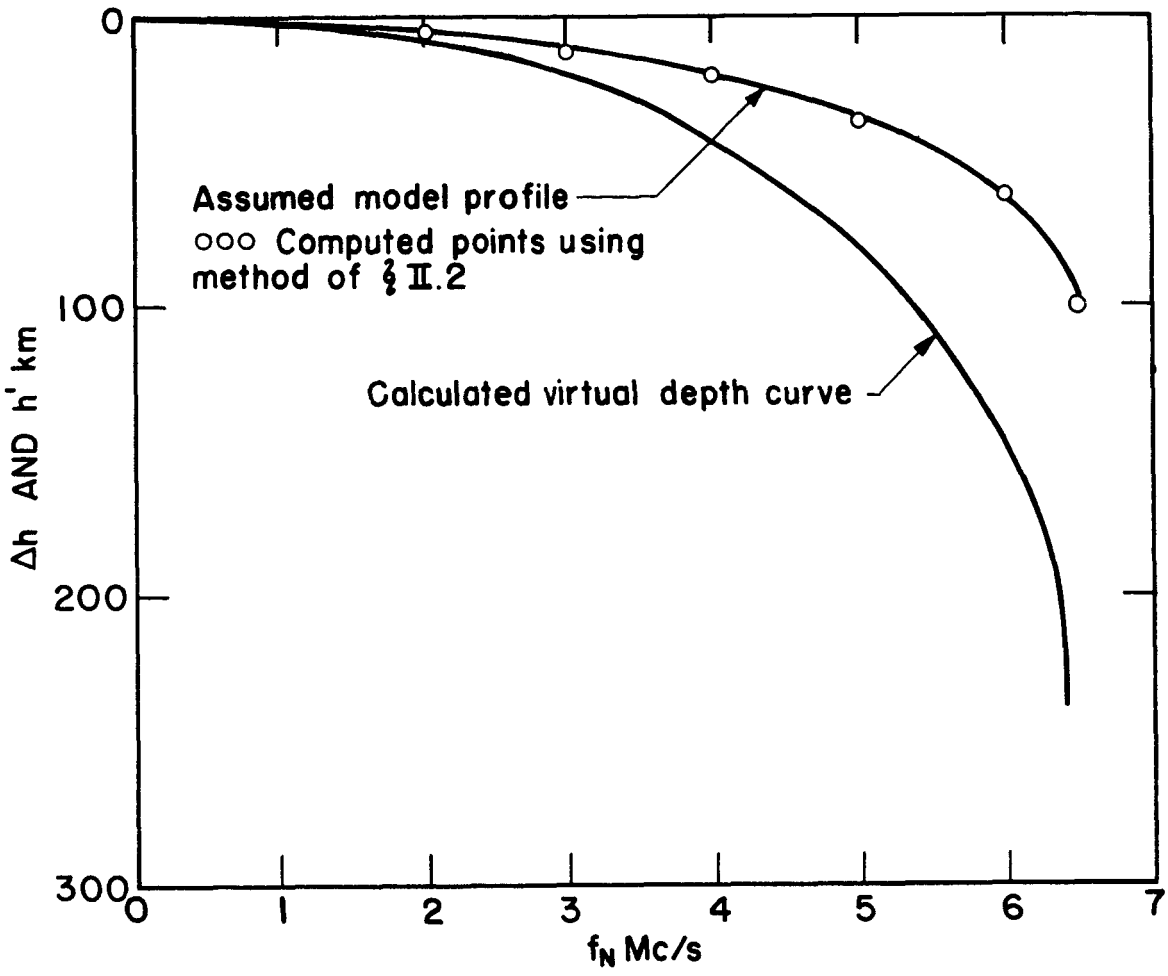

Figure 2: Test of the method of II.2, (parabolic model). The upper, continuous line represents the assumed topside electron density model. The lower, broken curve is the corresponding Ordinary ray h'(f) curve calculated for the no-field case. The circles represent the points computed by the technique described in the paper. It will be seen that the original profile can be recovered accurately.

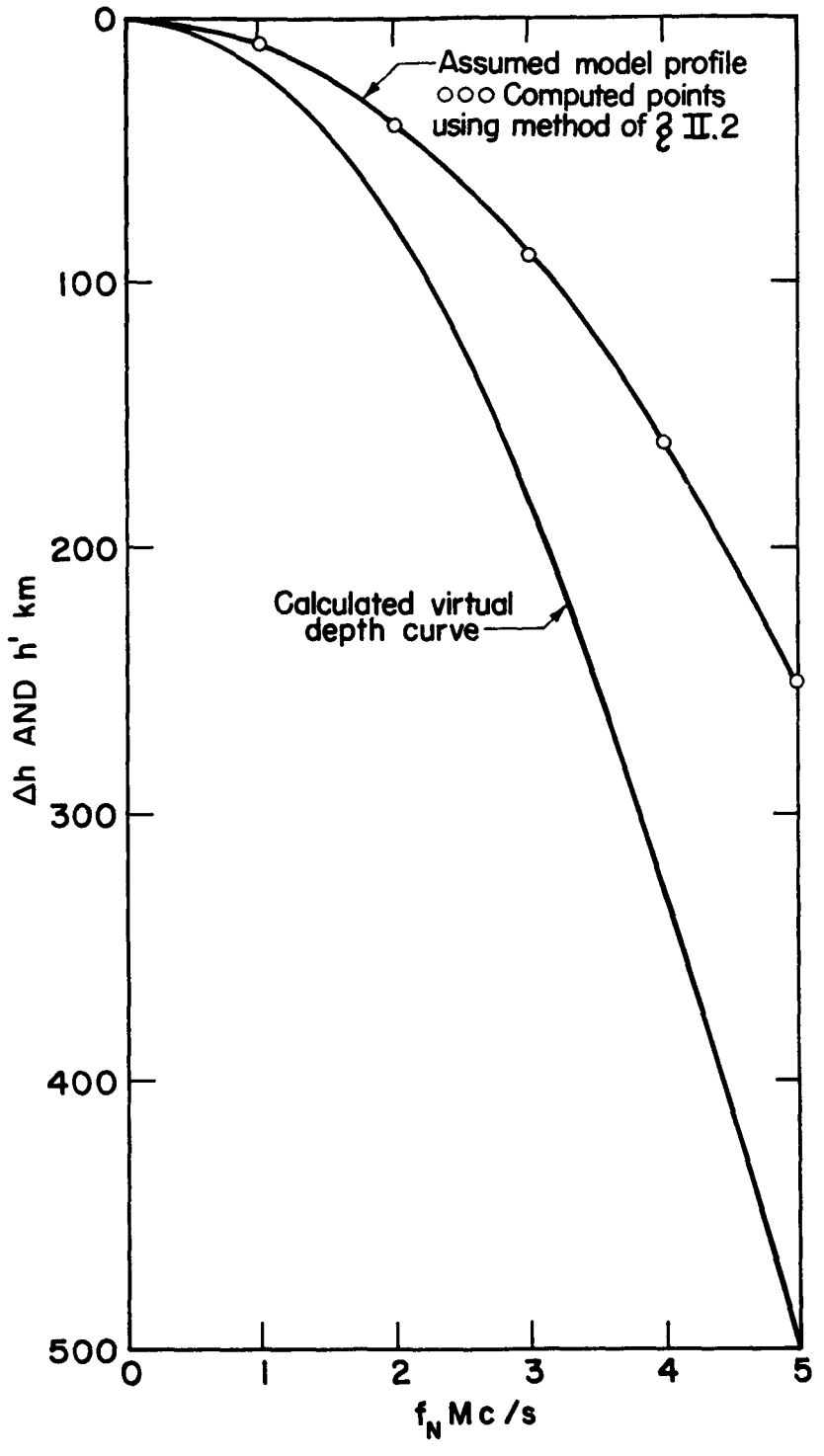

Figure 3: Test of the method of II.2, (square law model). The upper, continuous line represents the assumed topside electron density model. The lower, broken curve is the corresponding Ordinary ray h'(f) curve calculated for the no-field case. The circles represent the points computed by the technique described in the paper. It will be seen that the original profile can be recovered accurately.

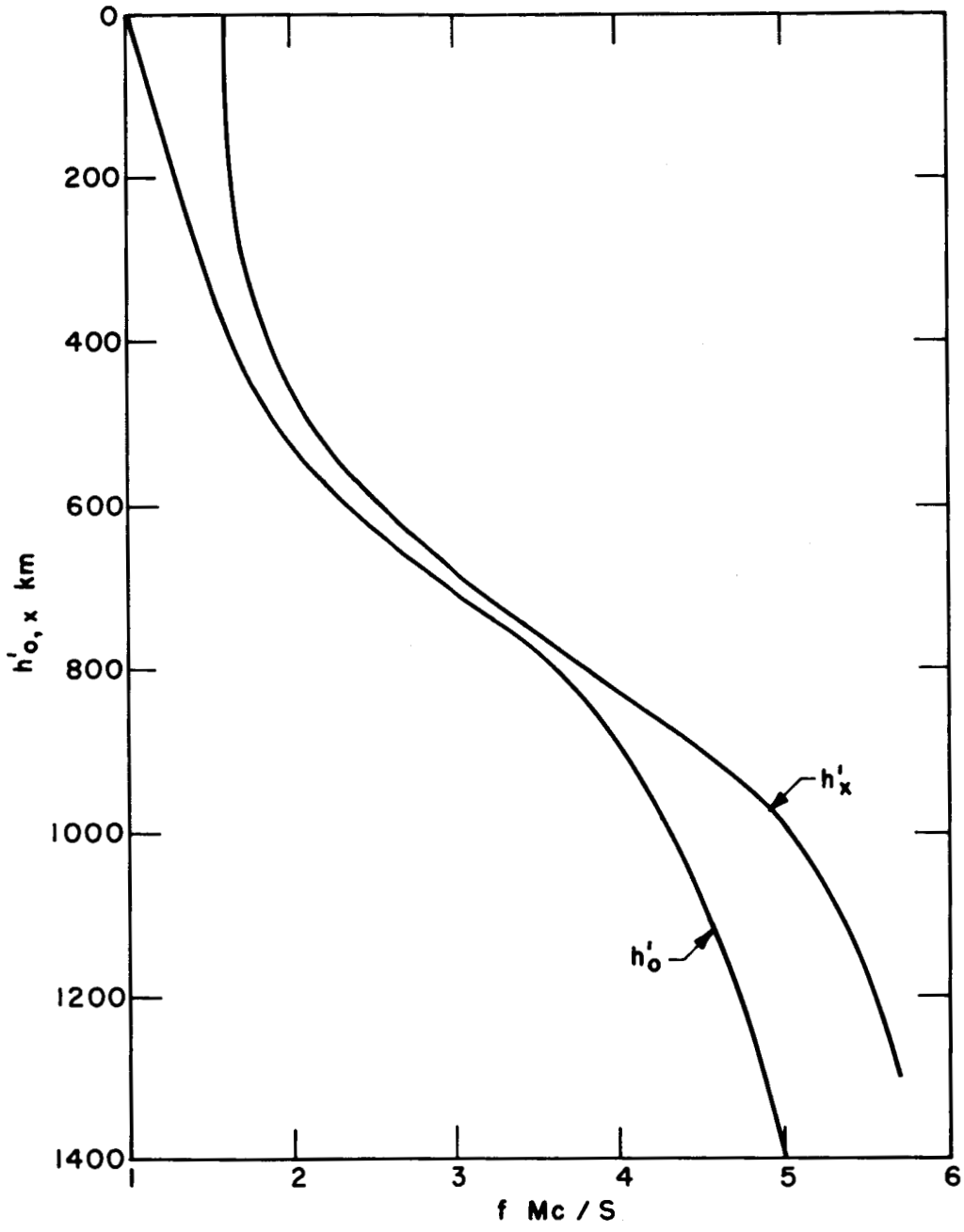

Figure 4. The Ordinary and Extraordinary ray virtual depth curves calculated for $I = 60^{\circ}$ $f_H = 0.9686$ Mc/s for the Chapman model (equation 34) used by Dougnik (1963).

figure 5. The parameters used in the calculation were:

f_c = 5.05 Mc/s

h_{max} = 250 km (above ground)

H = 100 km

I = 60^o

f_H (at the satellite) = 0.9686 Mc/s

The calculated points are seen to be on the assumed initial profile, indicating that the calculation satisfactorily recovers the assumed known $f_N(h)$ curve, for both the Ordinary and Extraordinary rays.

For the case of the Extraordinary ray, care must be taken to provide adequately for the variation of f_H with height. This problem is discussed in Appendix VI.

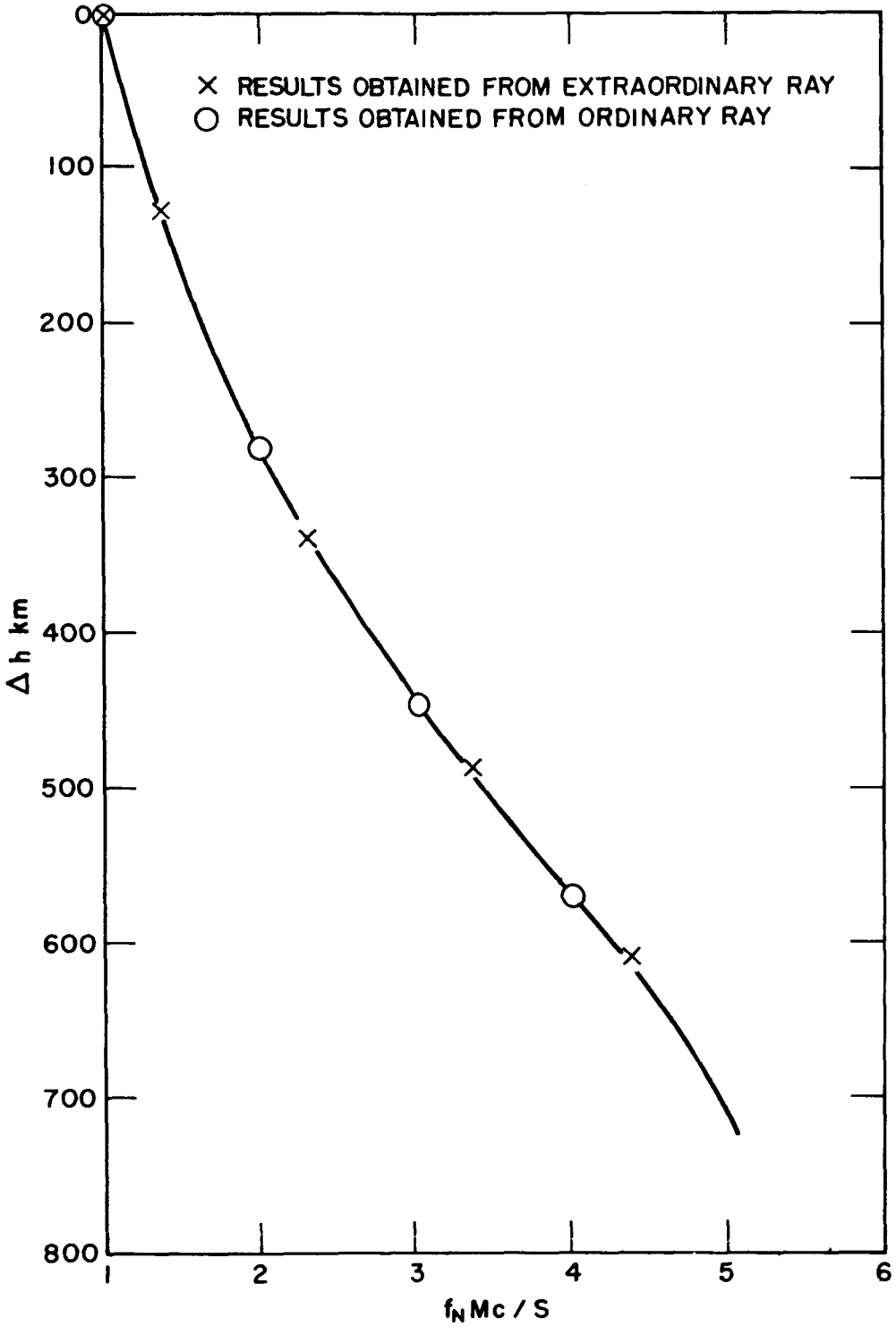

Figure 5. The Chapman model real-height profile used by Doupnik (1963) is shown as a continuous line. The calculated real heights obtained by the method of II.2 using the Ordinary and Extraordinary rays are shown by circles and crosses respectively. The errors between the calculated points and the true profile are in large measure due to the inability to make accurate height-frequency measurements from the small figures in the Doupnik report.

IV.2. Tests of the order of the polynomial to be used

If the order of the polynomial employed to describe the N(h) profile is too high, then oscillations will occur in the derived curve, and these will be unrelated to any actual changes in slope which may be present in the ionospheric profile. It is therefore desirable to investigate the order of the polynomial which will give the desired accuracy. Such an investigation for the case of an exponential profile is described below.

The model used is defined by

$$f_N^2 = f_o^2 \, e^{\Delta h/H} \tag{35}$$

with f_o = 1 Mc/s and H = 100 km. The corresponding virtual depths are given by

$$h' = 2H \, \text{sech}^{-1} \frac{f_o}{f} \tag{36}$$

The effect of varying the order, n, of the polynomial

$$\Delta h = \sum_{j=1}^{n} \alpha_j (f_N - f_o)^j \tag{37}$$

is investigated for the model above and the results presented in Table II.

It should be noted that the numbers given in the last column of Table II are calculated as percentages of the real depth, Δh, and not of the altitude, h, above the ground. Assuming h_o = 1000 km, the real height percentage error is always less than the value indicated in the last column. For example, in the first row of Table II below, the real height percentage error would be approximately 1.6/4 = 0.4%. The fourth column gives Δh calculated by the method of Thomas, Long and Westover (1963) as described in this report and referred to as T.L. & W. The

fifth column gives the difference

$$D = \Delta h(\text{model}) - \Delta h(\text{T.L. \& W.}).$$

The sixth column gives

$$D/\Delta h_{(\text{model})} \times 100\%$$

It is clear from an examination of the magnitude of the quantity, D, and of the % errors given in the last column of Table II that values of n=4, 5, 6, 7, or 8 give the best results. Thus, for the case of the topside ionosphere in which the electron density distribution is believed to be exponential in form, the profile may be derived to a high degree of accuracy by using, say, a polynomial of order 4 to 8.

IV.3. Investigation of errors due to inaccuracies in reading the h'(f) records

In practice, it is likely that the most serious errors which will arise in the N(h) calculation will derive from the fact that observations of the virtual height and frequency will contain random errors due to inaccuracies in reading h' and f from the experimental records. It is important to investigate, particularly in the case of the single polynomial method, the effects of including random errors of this kind.

In order to illustrate the effect of such errors, the h'(f) profile of Fig. 1 was perturbed in the following manner: Five sets of random numbers were generated, each set containing five numbers, corresponding to the five sample points on the h'(f) curve, each random number, R_N, in each set, having the property $|R_N| \leq 10$ km. The five numbers in each set were then algebraically added to the true value of h' at the corresponding sample frequency, f, and the five perturbed

h'(f) curves converted to h(f) curves. Table III shows the five sets of random numbers used in the perturbation, and Table IV, in conjunction with Fig. 6, summarizes the effect of the erroneous readings, taken on the h'(f) curve, on the resultant h(f) curve.

Secondly, an observed h'(f) curve for the location of Stanford was taken and this curve was sampled in a number of different ways. The effect of applying a single polynomial of order 6 in which two different sets of h' data points chosen along the curve were used is illustrated in Fig. 7. It is quite clear that, in practice, for most purposes in which a rough comparison of profiles at widely spaced locations on the earth is desirable, it is probably sufficiently accurate to use a single polynomial method with order 4, 5, 6, or 7. If, however, special attention is to be paid to the "kinks" which may occur in the topside profile, then it is best to use the overlapping polynomial method even though this involves rather more readings from the h'(f) curve (Thomas and Westover 1963). In Fig. 8, the profiles obtained from an observed topside ionogram using the single polynomial method in which both the Ordinary and Extraordinary rays have been converted to give electron density data are shown. It is seen that the results obtained from both curves agree.

TABLE II

	f_i Mc/s	h'_i km	Δh_i (model)	Δh_i (TL&W)	D km	%
n=4	2	526.78	277.25	272.78	4.46	1.60
	3	705.09	439.44	437.73	1.70	.38
	4	825.37	554.51	552.80	1.70	.30
	5	916.97	643.77	643.18	.58	.09
n=5	2	526.78	277.25	273.97	3.27	1.18
	3	705.09	439.44	438.05	1.38	.31
	4	825.37	554.51	553.32	1.18	.21
	5	916.97	643.77	643.01	.75	.11
	6	991.15	716.70	715.66	1.03	.14
n=6	2	526.78	277.25	274.71	2.53	.91
	3	705.09	439.44	438.30	1.13	.25
	4	825.37	554.51	553.60	.90	.16
	5	916.97	643.77	643.09	.67	.10
	6	991.15	716.70	716.05	.64	.08
	7	1053.56	778.36	777.97	.38	.04
n=7	2	526.78	277.25	275.21	2.03	.73
	3	705.09	439.44	438.49	.94	.21
	4	825.37	554.51	553.78	.72	.12
	5	916.97	643.77	643.22	.54	.08
	6	991.15	716.70	716.23	.46	.06
	7	1053.56	778.36	777.94	.41	.05
	8	1107.46	831.77	831.39	.37	.04

TABLE II (continued)

	f_i Mc/s	h'_i km	Δh_i (model)	Δh_i (TL&W)	D km	%
n=8	2	526.78	277.25	275.57	1.67	.60
	3	705.09	439.44	438.63	.80	.18
	4	825.37	554.51	553.90	.60	.10
	5	916.97	643.77	643.18	.58	.09
	6	991.15	716.70	716.05	.64	.08
	7	1053.56	778.36	777.69	.66	.08
	8	1107.46	831.77	831.81	-.04	-.00
	9	1154.90	878.88	877.75	1.12	.12
n=9	2	526.78	277.25	275.84	1.40	.50
	3	705.09	439.44	438.75	.68	.15
	4	825.37	554.51	553.89	.61	.11
	5	916.97	643.77	643.21	.55	.08
	6	991.15	716.70	715.07	1.62	.22
	7	1053.56	778.36	778.53	-.17	-.02
	8	1107.46	831.77	831.76	.00	.00
	9	1154.90	878.88	866.39	12.48	1.42
	10	1197.28	921.03	947.08	-26.05	-2.82
n=10	2	526.78	277.25	275.64	1.60	.57
	3	705.09	439.44	438.65	.78	.17
	4	825.37	554.51	554.00	.50	.09
	5	916.97	643.77	643.04	.72	.11
	6	991.15	716.70	716.82	-.12	-.01
	7	1053.56	778.36	780.96	-2.60	-.33
	8	1107.46	831.77	822.72	9.04	1.08
	9	1154.90	878.88	885.95	-7.07	-.80
	10	1197.28	921.03	905.26	15.76	1.71
	11	1235.58	959.15	1047.05	-87.90	-9.16

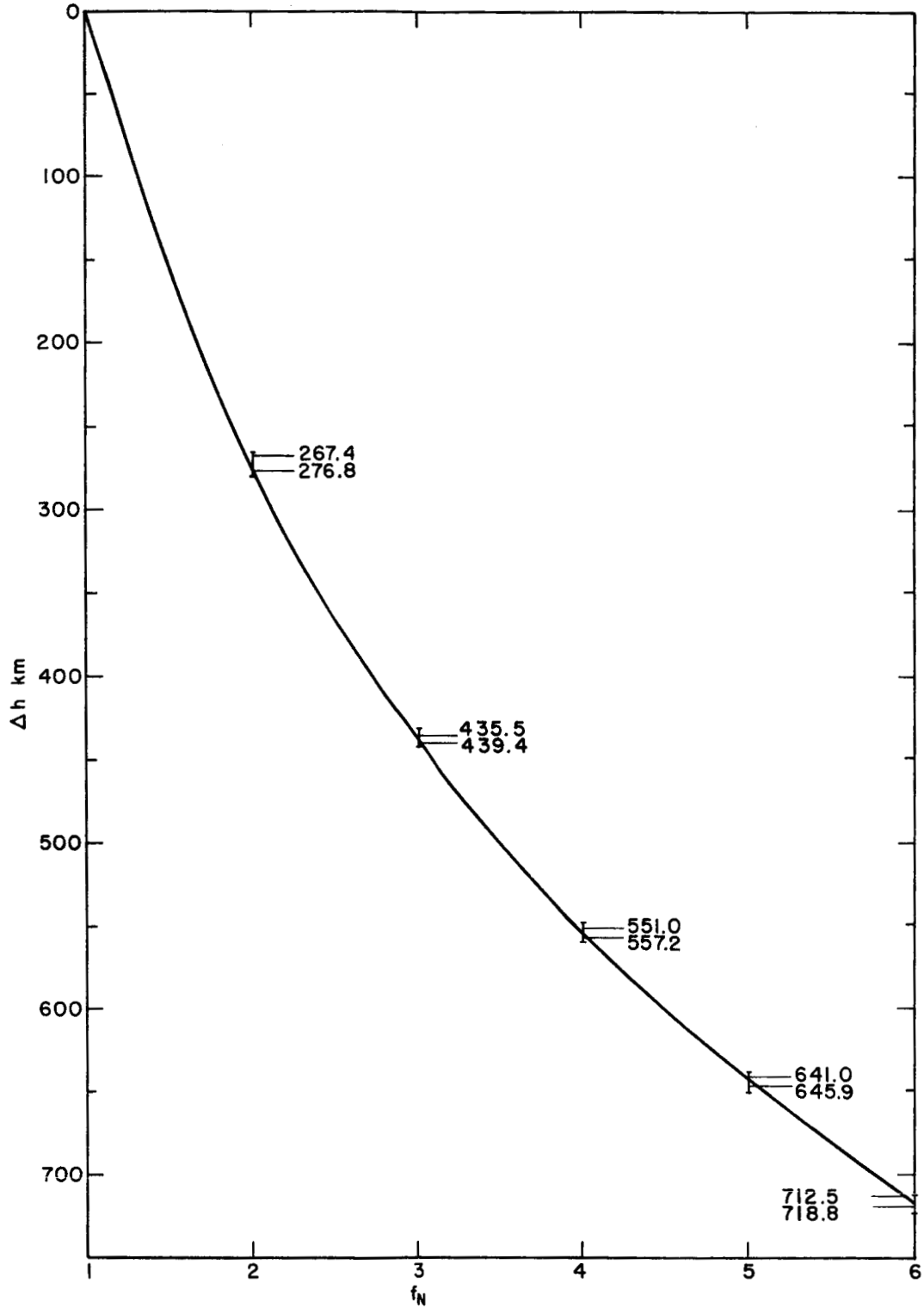

Figure 6. To illustrate the accuracy of the method. The effect upon the computed real heights of introducing random errors into the h'(f) curve of Fig. 1 is indicated in the diagram. The magnitude of the random errors appear in Table III and the tabulated Δh results appear in Table IV.

TABLE III

Sample Frequency	Amount of error (km.) to be introduced at the sample frequency				
	Error 1	Error 2	Error 3	Error 4	Error 5
2.0	-0.691	-3.946	-1.958	3.059	-3.100
3.0	-3.027	4.070	5.308	-0.346	-4.314
4.0	6.396	-4.512	8.966	-2.846	2.041
5.0	-1.360	4.423	-0.160	-7.491	9.639
6.0	9.636	6.979	0.212	-5.065	4.562

Table III. Five sets of random numbers which were algebraically added to the virtual height profile of Fig. 1 to obtain 5 perturbed h(f) profiles.

TABLE IV

Sample Frequency	True h(f) Profile	Error in Profile1	Error in Profile 2	Error in Profile 3	Error in Profile 4	Error in Profile 5
2.0	273.976	2.781	2.469	-1.429	2.528	-1.014
3.0	438.059	-0.633	-1.156	0.846	1.348	-2.588
4.0	553.324	1.889	-2.310	3.862	0.034	-1.286
5.0	643.009	1.691	-1.425	2.863	-1.973	2.006
6.0	715.665	1.288	2.503	0.870	-3.181	3.117

Table IV. The true h(f) profile corresponding to the h'(f) curve of Fig. 1, together with the errors resulting in the h(f) profile due to random errors in reading the h'(f) curve.

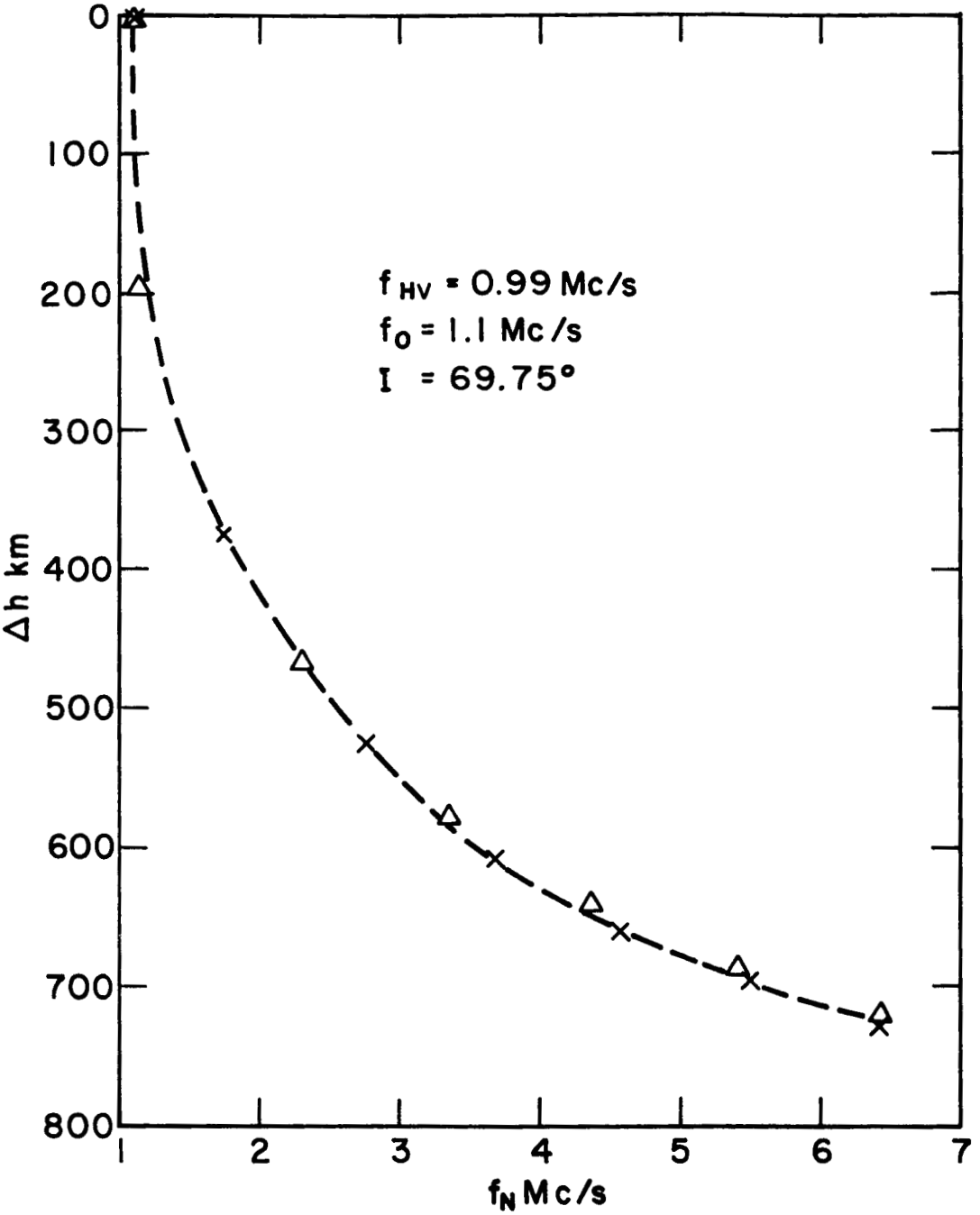

Figure 7. Topside N(h) profile deduced from Alouette observations made at Stanford at 20.52.23 GMT on 7 December 1962. The real height electron density distribution is plotted in the form of a curve of Δh, against plasma frequency where Δh is the real depth of reflection below the vehicle.

X Results obtained from one set of extraordinary ray samples
Δ Results obtained from a second set of extraordinary ray samples taken from the same $h'_X(f)$ curve

V. Some typical results showing N(h) profiles deduced from observed Alouette topside soundings recorded at Stanford

V.1. Daytime observations:

The main feature of daytime profiles observed near Stanford is that on most occasions the curves are quite smooth and contain no kinks corresponding to abrupt changes of slope in the N(h) profile. Examples of such profiles reduced by the method described in this report were shown in Figs. 7 and 8. The ionogram used for this reduction is shown in Fig. 9. The form of the $h'(f)$ curves at night, however, is quite different and it is usually observed that a very large cusp referred to as f_{bx} occurs on the Extraordinary ray trace. Some examples of these curves are shown in Fig. 10. It is shown in the next section that the night-time curves assume this shape as a natural consequence of the behavior of the refractive index for the Extraordinary ray whenever the plasma frequency near the vehicle approaches the gyro-frequency for electrons. Curves illustrating the behavior of the Ordinary ray refractive index for a variety of conditions are given in Appendix III and may be compared with the corresponding curves for the Extraordinary ray also given in that Appendix.

V.2. The form of the topside ionograms at night

Figure 11 shows Extraordinary ray topside ionograms calculated in the manner described in Appendix V for a series of exponential models given by (28) so that

$$f_N^2 = f_o^2 \, e^{-\frac{h}{200}}$$

where, as before, h is the real height measured from the ground, f_N is the plasma frequency and f_o the value of f_N at the vehicle. In these models, f_o was given a series of different values so that the form of the topside $h'_x(f)$ curve could be examined as f_o approached the gyro-frequency for electrons.

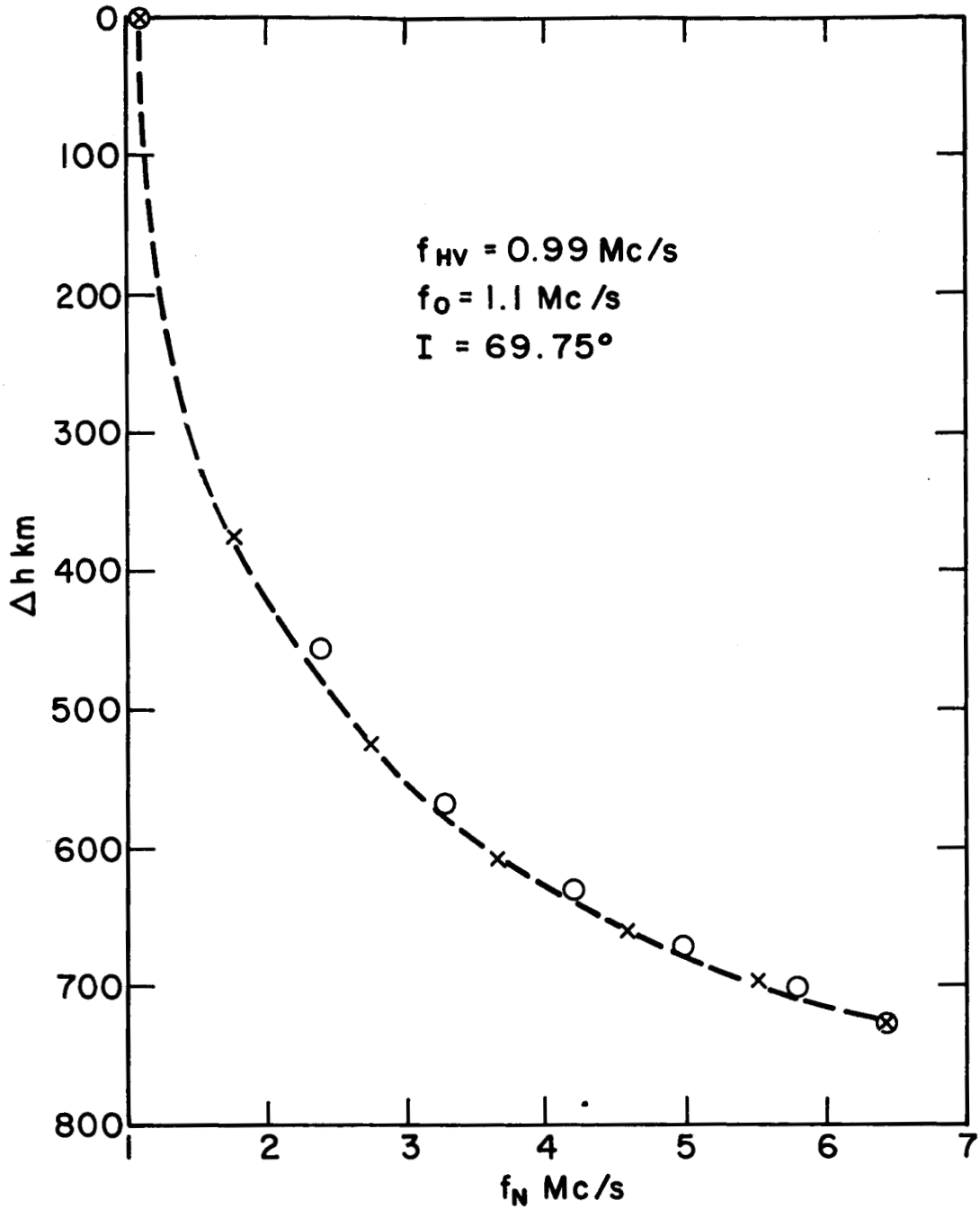

Figure 8. Topside N(h) profile deduced from Alouette observations made at Stanford at 20.52.23 GMT on 7 December 1962. The real height electron density distribution is plotted in the form of a curve of Δh, against plasma frequency where Δh is the real depth of reflection below the vehicle.

X Results obtained from a set of extraordinary ray samples
O Results obtained from a set of ordinary ray samples from the same ionogram

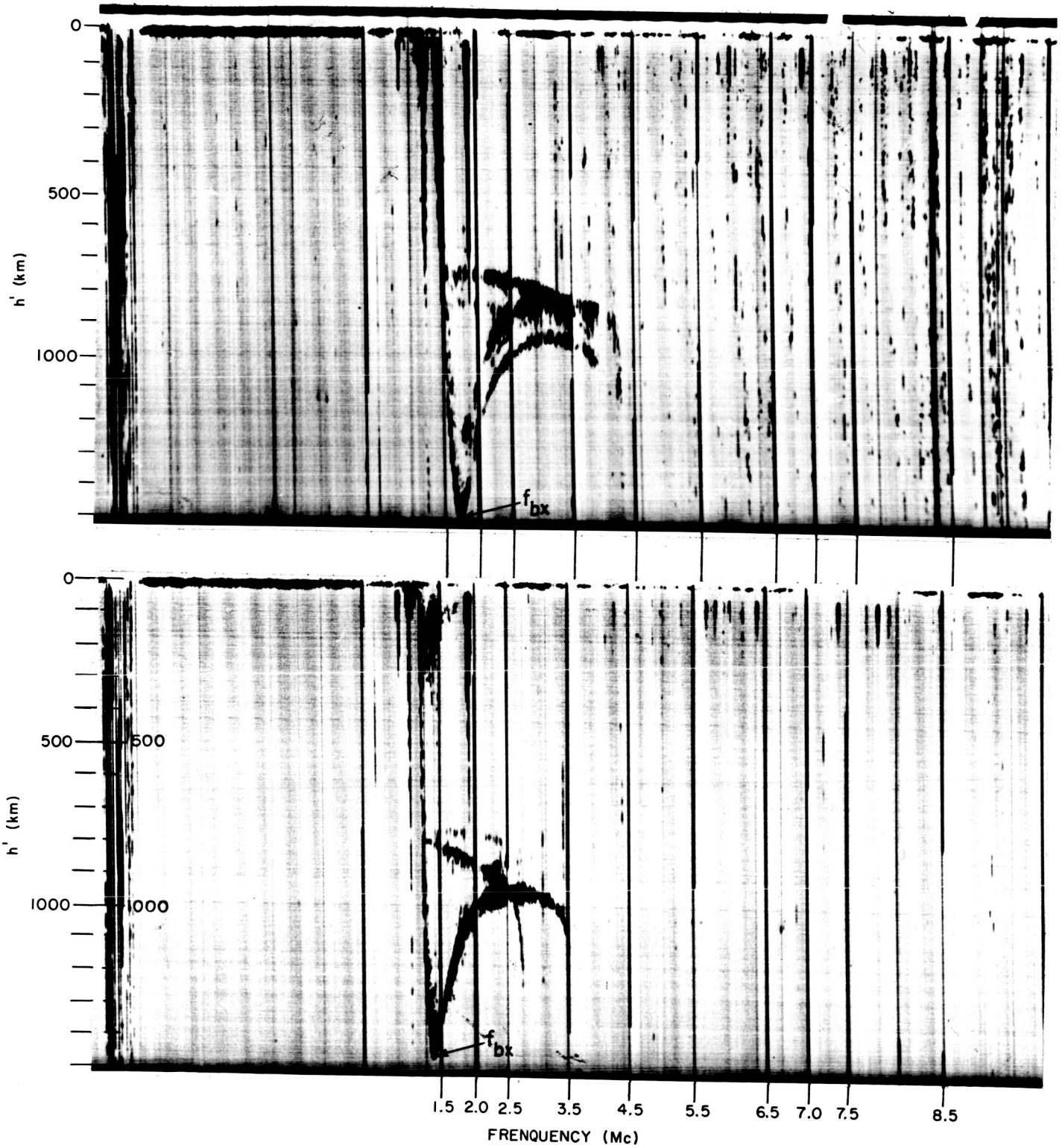
0
500
1000
h' (km)
f_{bx}
0
500
1000
500
1000
h' (km)
f_{bx}
1.5 2.0 2.5 3.5 4.5 5.5 6.5 7.0 7.5 8.5
FRENQUENCY (Mc)

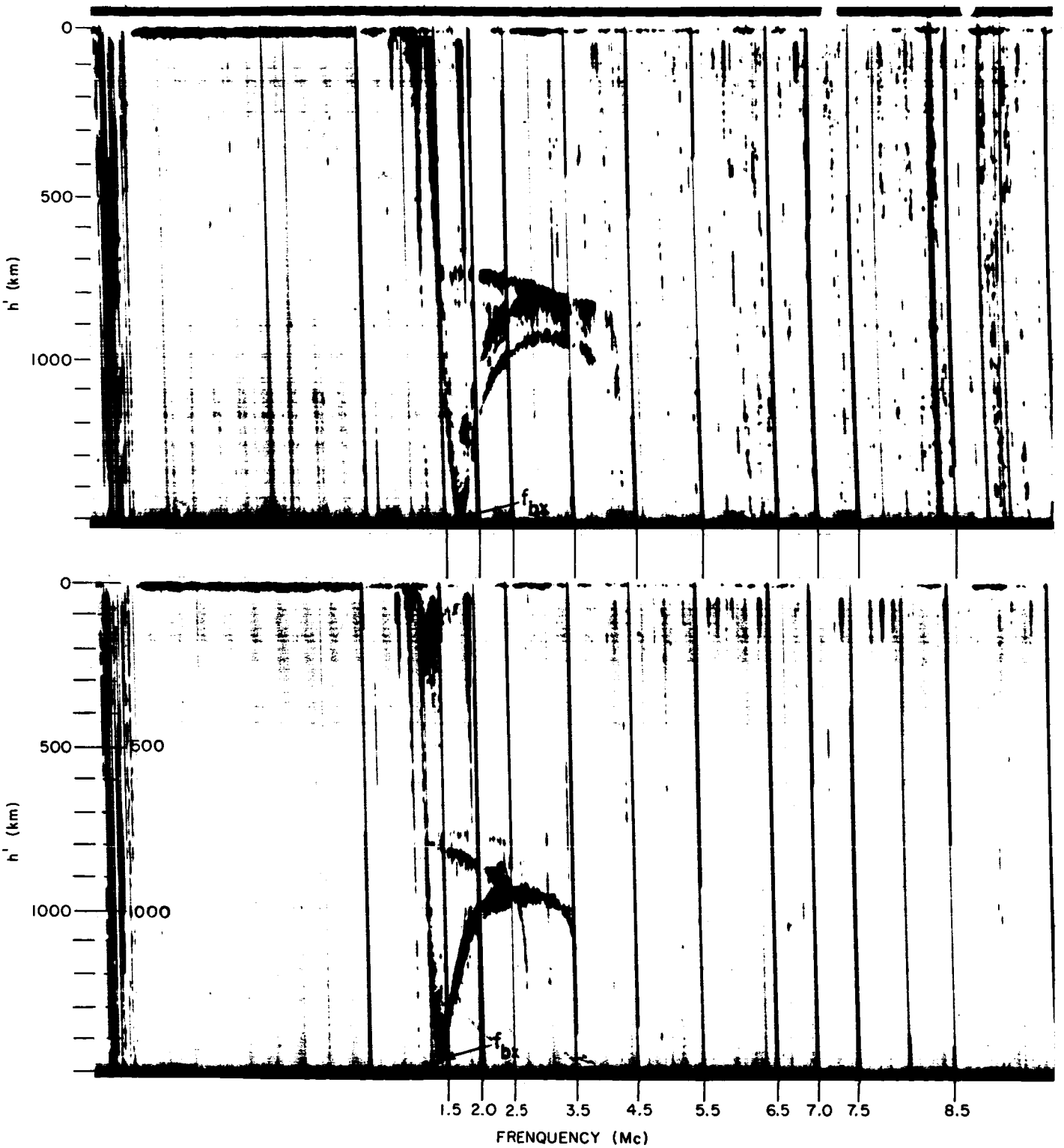
0
500
1000
h' (km)
f_{bx}
0
500
1000
h' (km)
f_{bx}
1.5 2.0 2.5 3.5 4.5 5.5 6.5 7.0 7.5 8.5
FRENQUENCY (Mc)

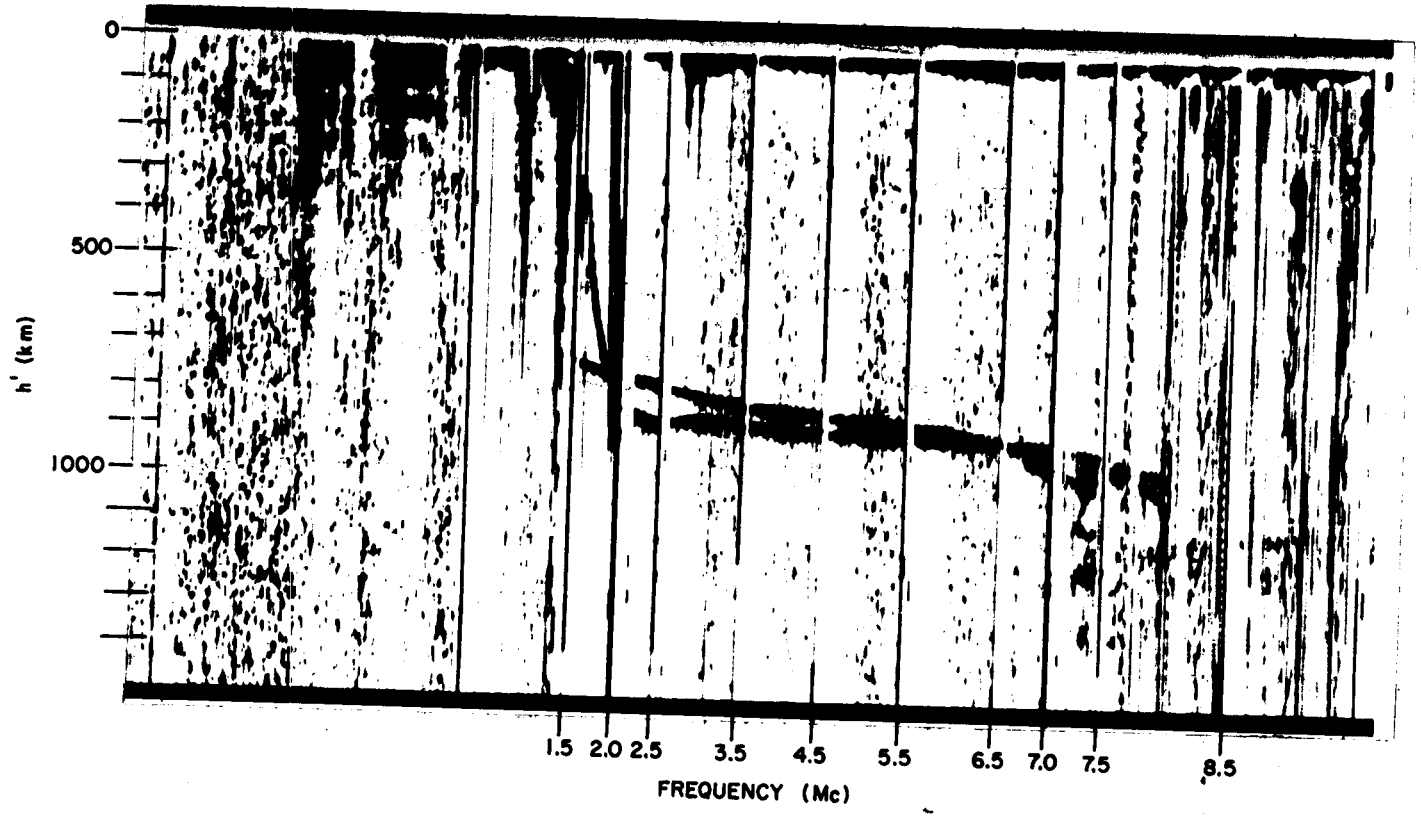
0
500
1000
h' (km)
1.5
2.0
2.5
3.5
4.5
5.5
6.5
7.0
7.5
8.5
FREQUENCY (Mc)

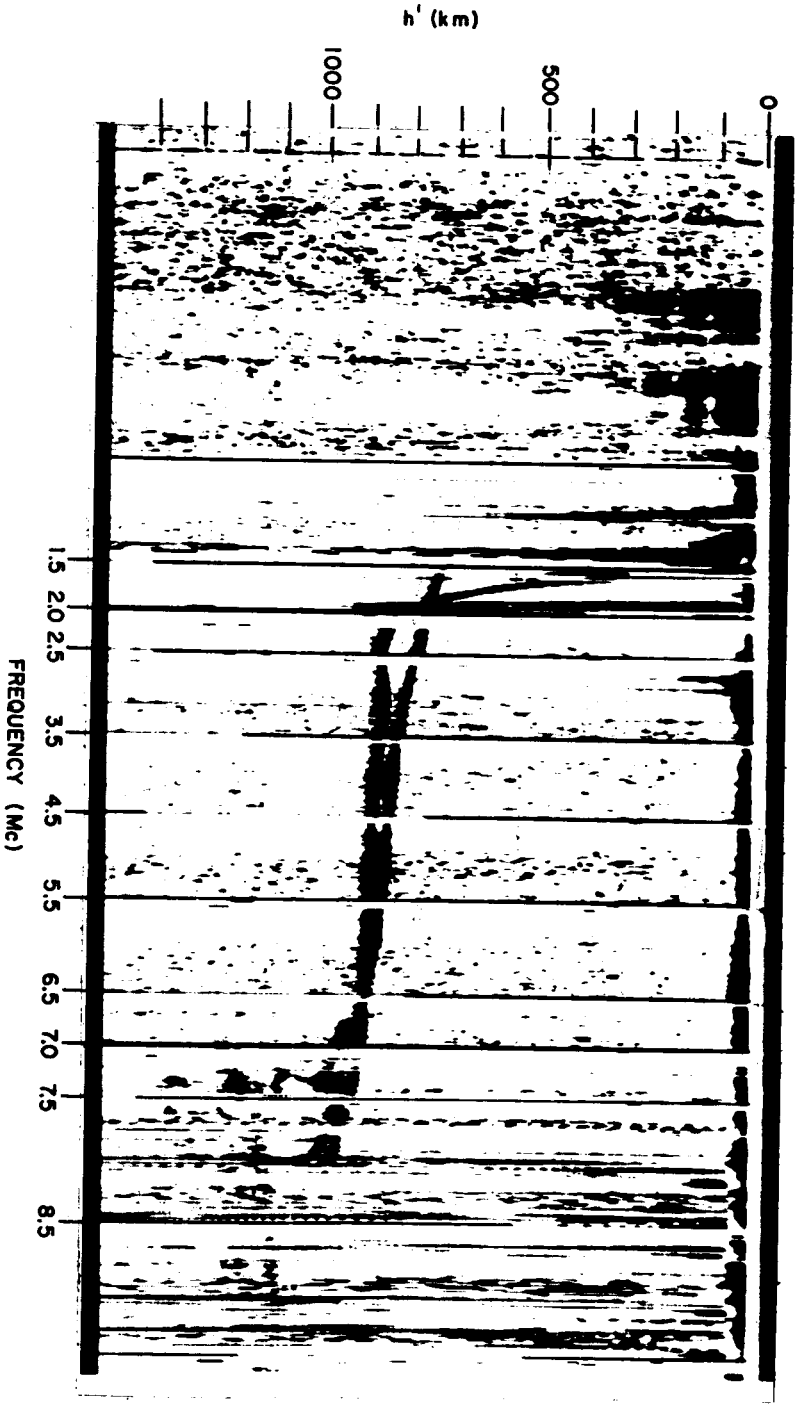
h' (km)
1000
500
0
FREQUENCY (Mc)
1.5
2.0
2.5
3.5
4.5
5.5
6.5
7.0
7.5
8.5

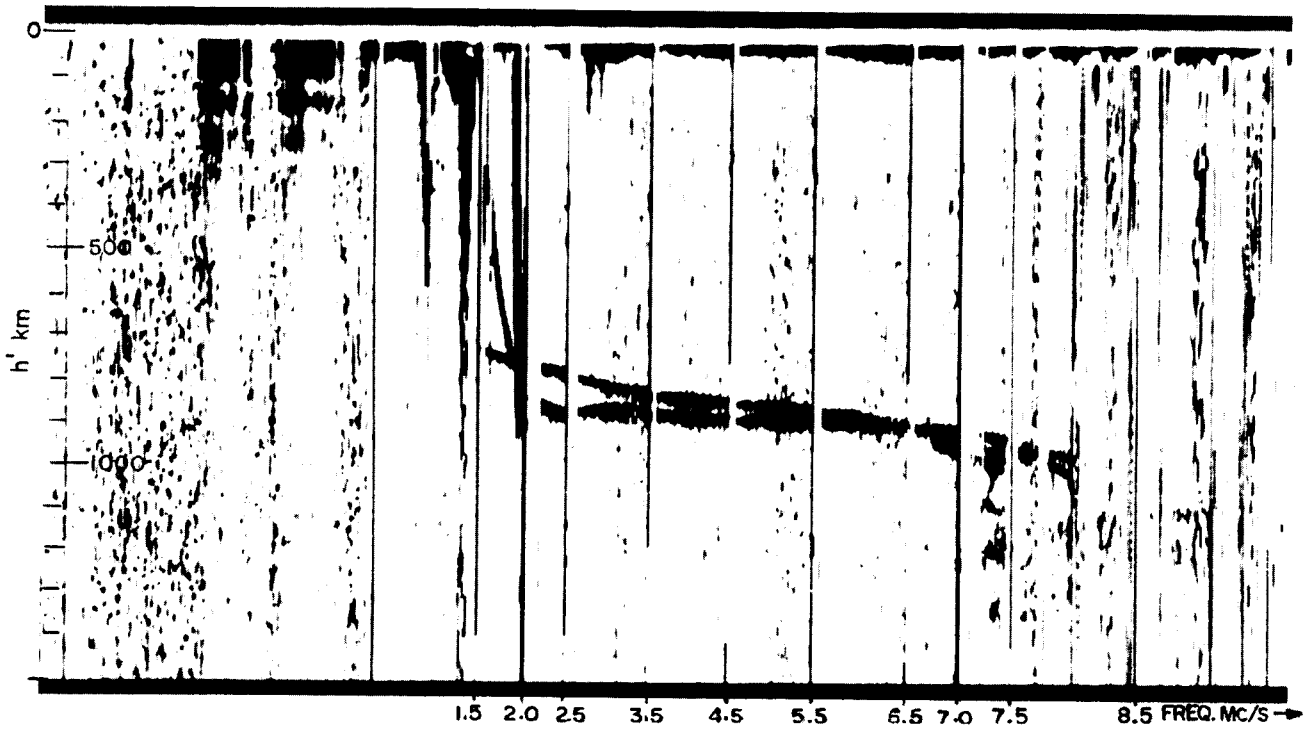

Figure 9. An example of a typical daytime Alouette topside ionogram as received at Stanford. This is the ionogram which was sampled to produce the results in Figs. 7 and 8. Pass No. 950. 7 December 1962, 20.52.23 GMT.

Figure 10: Examples of typical night-time Alouette topside ionograms as received at Stanford. The portion labeled f_{bx} on the ionograms is the "cusp" on the Extraordinary ray referred to in the text. Note the normal behavior of the Ordinary ray. Pass No. 3726, 29 June 1963, 06.44.34 GMT; Pass No. 3658, 24 June 1963, 07.07.55 GMT.

In order to compute $h'_x(f)$ the procedure described in Appendix V was used. This involves the evaluation of the following integral in which $a=(1-f_v^2/f_R^2)^{\frac{1}{2}}$

$$h'_x(f) = 2H\int_{t_R=o}^{t_R=a} \frac{G_R}{x_R}\, dt_R$$

An examination of the G_R/x_R versus t_R curves corresponding to the Extraordinary ray curves shown in Appendix III indicates that as the plasma frequency at the vehicle approaches the gyro-frequency for electrons the area under the appropriate curve first increases rapidly, then decreases (producing the cusp f_{bx} of Fig. 10) before increasing again corresponding to the infinity in the $h'_x(f)$ curve at the critical frequency of the layer. Thus, a cusp is obtained in the $h'_x(f)$ curve even though there is no cusp or sudden change of slope in the N(h) profile. Figure 11 shows that as the electron density falls at the level of the satellite from its daytime value to typical night-time values, that is, as the plasma frequency at the vehicle approaches the gyro-frequency, the form of the h'(f) curve changes from the smooth type of variation observed in the daytime to the cusp structure already shown in Fig. 10. The frequency at which the cusp occurs and the virtual depth at this frequency depend on the relative magnitudes of the plasma frequency at the vehicle and the gyro-frequency as well as on the absolute magnitude of the gyro-frequency and the dip angle, although the dependence on the latter is not marked as is shown in curves in Fig. 12. It is clear from the analysis presented immediately above that it would be wrong to interpret observations of the kind shown in Fig. 10 as indicating a kink in the N(h) profile unless the frequency at which the E-ray has zero range is well above the gyro-frequency. The daytime kinks corresponding to field aligned ledges of ionization are quite different in form from the kinks referred to in the night-time ionograms. These daytime kinks are illustrated in examples shown in a companion report (Thomas & Sader 1963).

Appendix V describes the technique used to synthesize the theoretical h'(f) curves shown in Figs. 11 and 12.

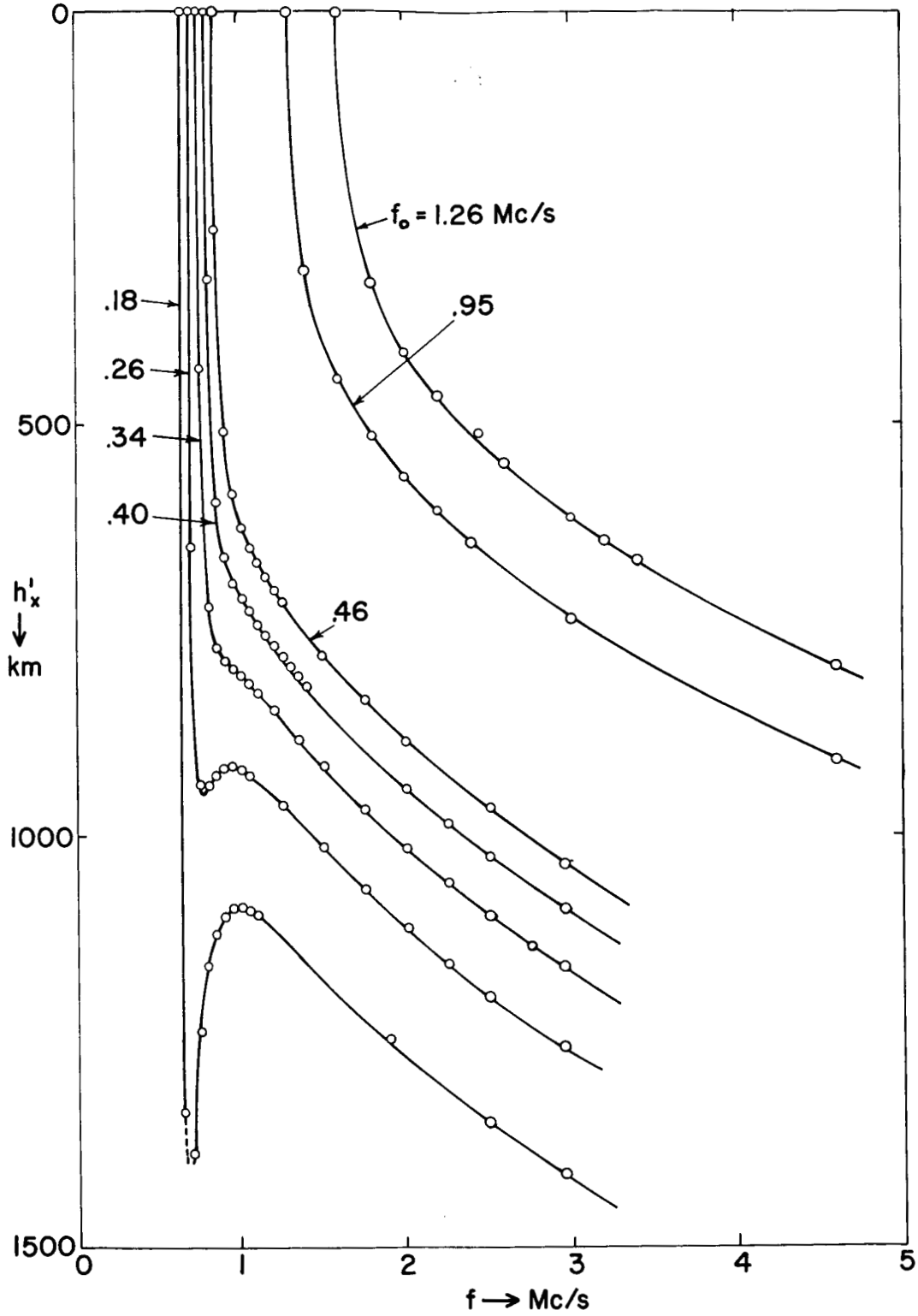

Figure 11: Analytically synthesized topside $h'_x(f)$ curves for a series of assumed exponential profiles with a scale height of 200 km, calculated for a series of values of f_o with $I = 0^o$, and $f_{Hv} = 0.6$ Mc/s. The values of f_o are for typical daytime $h'_x(f)$ curves (f_o = 1.26, 0.95 Mc/s), transitional curves between night and day (f_o = .46, .40, .34 Mc/s) and typical night-time curves (f_o = .26, .18 Mc/s). Only the upper part of the $h'_x(f)$ curves are shown.

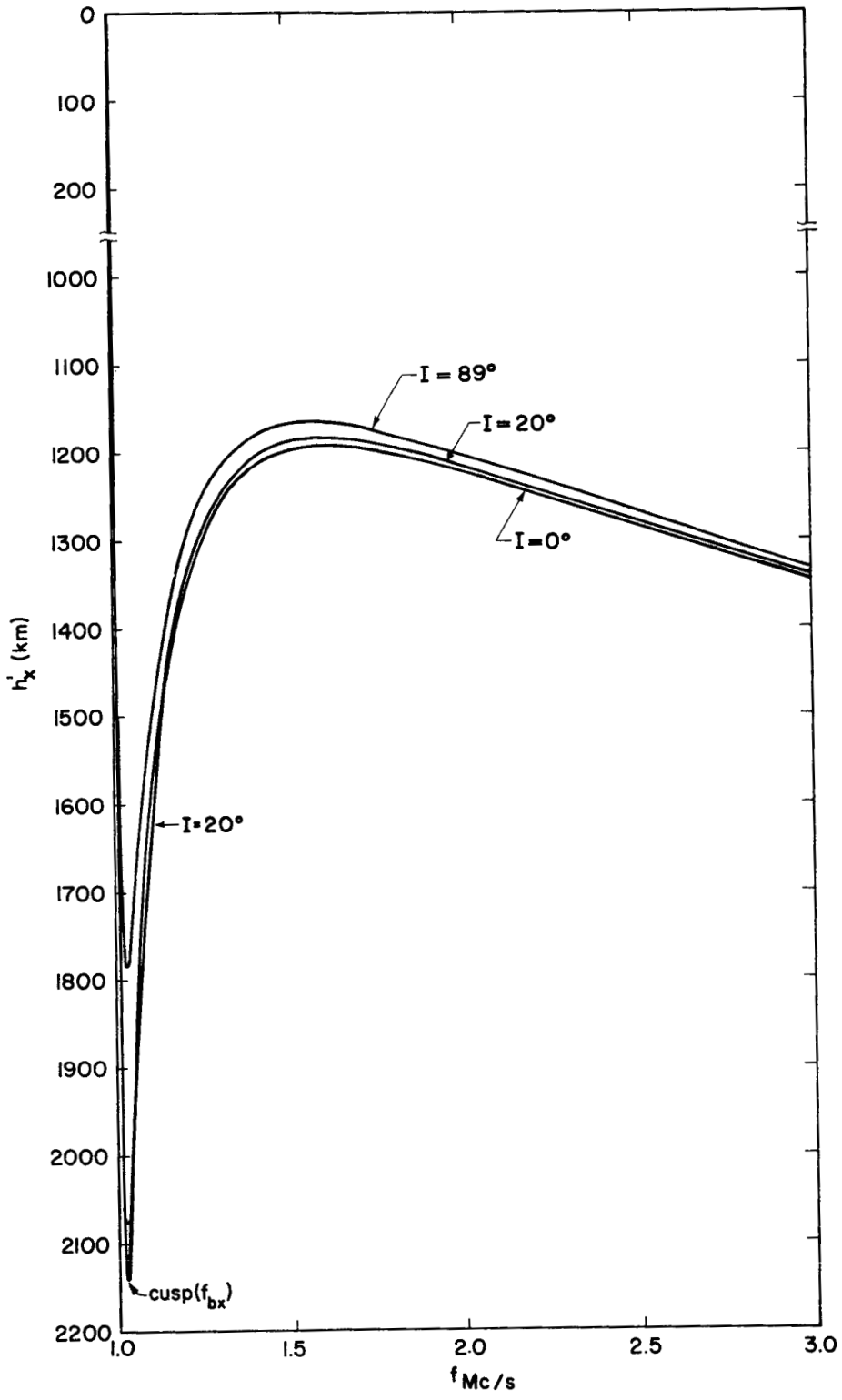

Figure 12: The dependence of the virtual depth at the cusp frequency, f_{bx}, on the $h'_x(f)$ trace of night time topside ionograms upon the magnetic dip angle, I, assuming an exponential N(h) distribution with a scale height of 200 km, and f_{Hv} = 0.95 Mc/s. f_{xv} = 1.0 Mc/s.

APPENDIX I

An alternative form of the solution of the $h'(f) - N(h)$ conversion problem for topside ionograms is given below:

We write

$$h = \sum_{j=o}^{n} \alpha'_j \, f_N^{\,j}$$

so that

$$h_o = \alpha'_o + \alpha'_1 f_o + \alpha'_2 f_o^2 \ldots\ldots\ldots \alpha'_n f_o^n$$

$$h_1 = \alpha'_o + \alpha'_1 f_1 + \alpha'_2 f_1^2 \ldots\ldots\ldots \alpha'_n f_1^n$$

$$\vdots$$

$$h_n = \alpha'_o + \alpha'_1 f_n + \alpha'_2 f_n^2 \ldots\ldots\ldots \alpha'_n f_n^n$$

then writing $\alpha_n = -\alpha'_n$,

$$h_o - h_1 = \Delta h_1 = \alpha_1(f_1 - f_o) + \alpha_2(f_1^2 - f_o^2) + \ldots\ldots\ldots \alpha_n(f_1^n - f_o^n)$$

$$\vdots$$

$$h_o - h_n = \Delta h_n = \alpha_1(f_n - f_o) + \alpha_2(f_n^2 - f_o^2) + \ldots\ldots\ldots \alpha_n(f_n^n - f_o^n)$$

i.e.

$$\Delta h = \sum_{j=1}^{n} \alpha_j (f_N^j - f_o^j) \; ; \; \Delta h_o = o$$

This may be written in matrix form and, subsequently, a similar procedure adopted to the one described in Section II.2. The matrix $\underline{A}$ would again be an n by n matrix, but with a typical element $a_{ij} = (f_i^j - f_o^j)$ rather than $a_{ij} = (f_i - f_o)^j$.

The method presented in Section II.2. is likely to be more accurate, however, since for a given value of h', the coefficients a_{ij} would have to be computed to a very high order of accuracy if the form $a_{ij} = (f_i^j - f_o^j)$ is used.

The authors' attention has recently been drawn to an article by Knecht, van Zandt, and Watts (1962) in which a method similar to that outlined in this Appendix is suggested as a solution to the topside h'(f) to N(h) conversion problem.

APPENDIX II. CALCULATION OF THE MATRIX ELEMENTS b_{ij}

The calculation of the matrix elements b_{ij} involves the computation of the group refractive index μ'. This may be evaluated for the Ordinary and Extraordinary rays, for different magnetic conditions from the Appleton-Hartree magneto-ionic theory using standard procedures (see for example Thomas and Vickers 1959, Titheridge 1961).

$$b_{ij} = j\int_{f_o}^{f_i} \mu_o'(f_i,f_N)\ (f_N-f_o)^{j-1}\, df_N$$

substituting $\mu_o' = G_o/t = G_o/\sqrt{1-f_o^2/f_i^2}$

we have

$$b_{ij} = j\int_{f_o}^{f_i} \frac{G_o(f_N-f_o)^{j-1}}{\sqrt{1-\left(\frac{f_N}{f_i}\right)^2}}\, df_N$$

The integrand remains finite at the upper limit if the substitution $f_N = f_i \sin\theta$ is made, giving:

$$b_{ij} = j\, f_i \int_{\sin^{-1}(f_o/f_i)}^{\pi/2} G_o(f_i \sin\theta - f_o)^{j-1}\, d\theta$$

Similarly, the expression for b_{ij} in the case of the Extraordinary ray becomes

$$b_{ij} = j\, f_i' \int_{\sin^{-1}(f_o/f_i')}^{\pi/2} G_R(f_i' \sin\theta - f_o)^{j-1}\, d\theta$$

where the G_o and G_R are computed as described in Section III.

The numerical procedure for calculating the above integrals is carried out using Simpson's rule. The step size used in the integration is progressively halved until the difference between two successive values of the integral becomes less than a specified amount.

APPENDIX III. THE GROUP REFRACTIVE INDICES μ_o' AND μ_x'

In order to illustrate the behavior of the group refractive indices for the Ordinary and Extraordinary rays, μ_o' and μ_x' respectively, it is convenient to work in terms of the parameters G_o and G_R as functions of t_R* where

$$G_o = \mu_o' \, t_R$$

$$G_R = \mu_x' \, t_R$$

$$t_R = \sqrt{1 - (f_o/f)^2}$$

The equations for G_o and G_R are those presented in Section III. A variation of t_R from 0 to 1 implies a variation of f_o from f to 0.

In Figs. AIII.1 through AIII.18, these quantities are plotted for a series of values of magnetic dip angle, I.

The frequency f assumes a series of multiple values of f_H ranging from $4f_H$ to $0.5f_H$.

Footnote:

* As t (see p. 16) is equal to t_R for the ordinary ray, t_R is appropriate as a common parameter.

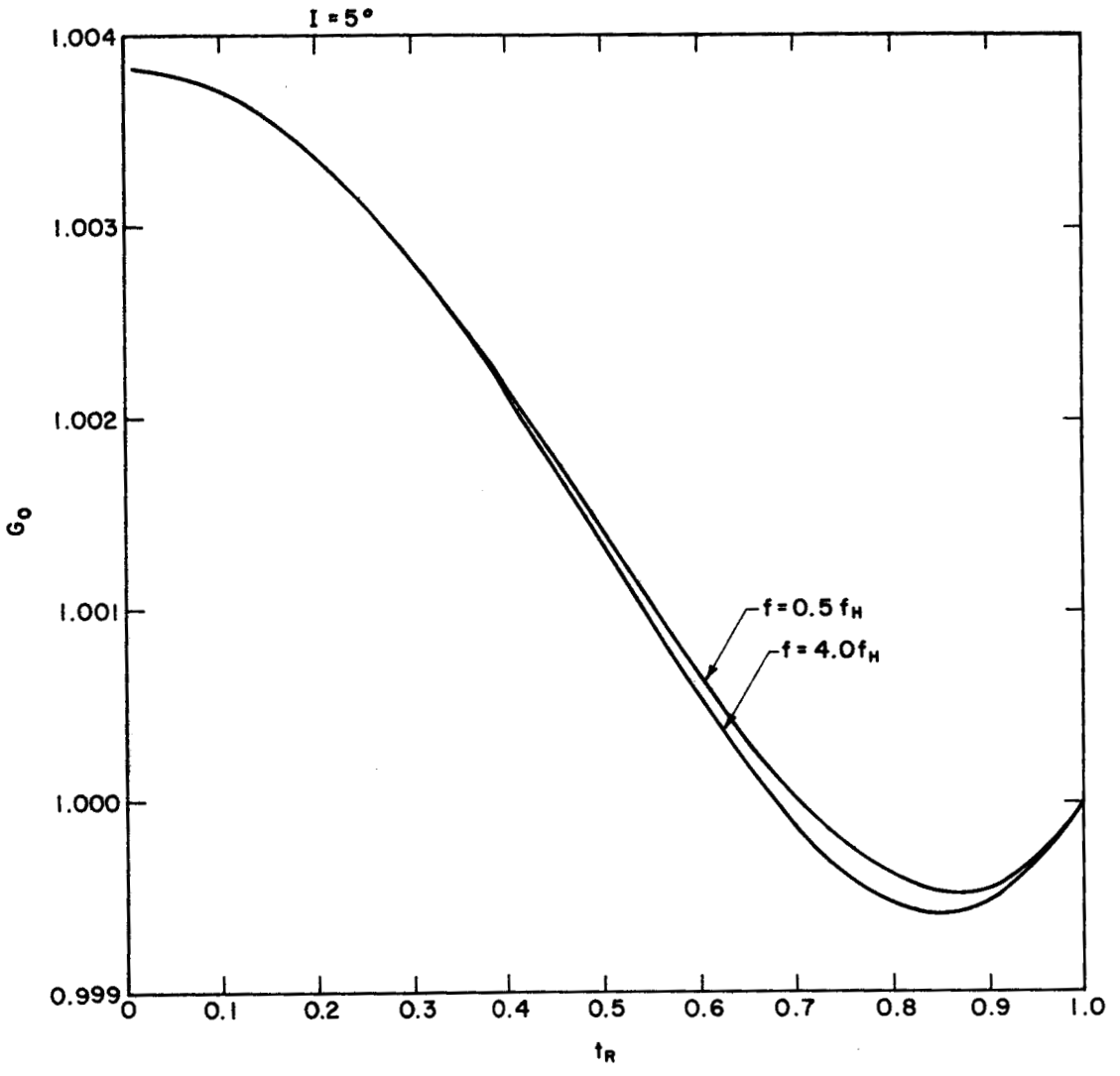

AIII.1 to AIII.6: To illustrate the behavior of the group refractive index for the Ordinary ray. For convenience, the quantity G_o is plotted versus t_R (see text).

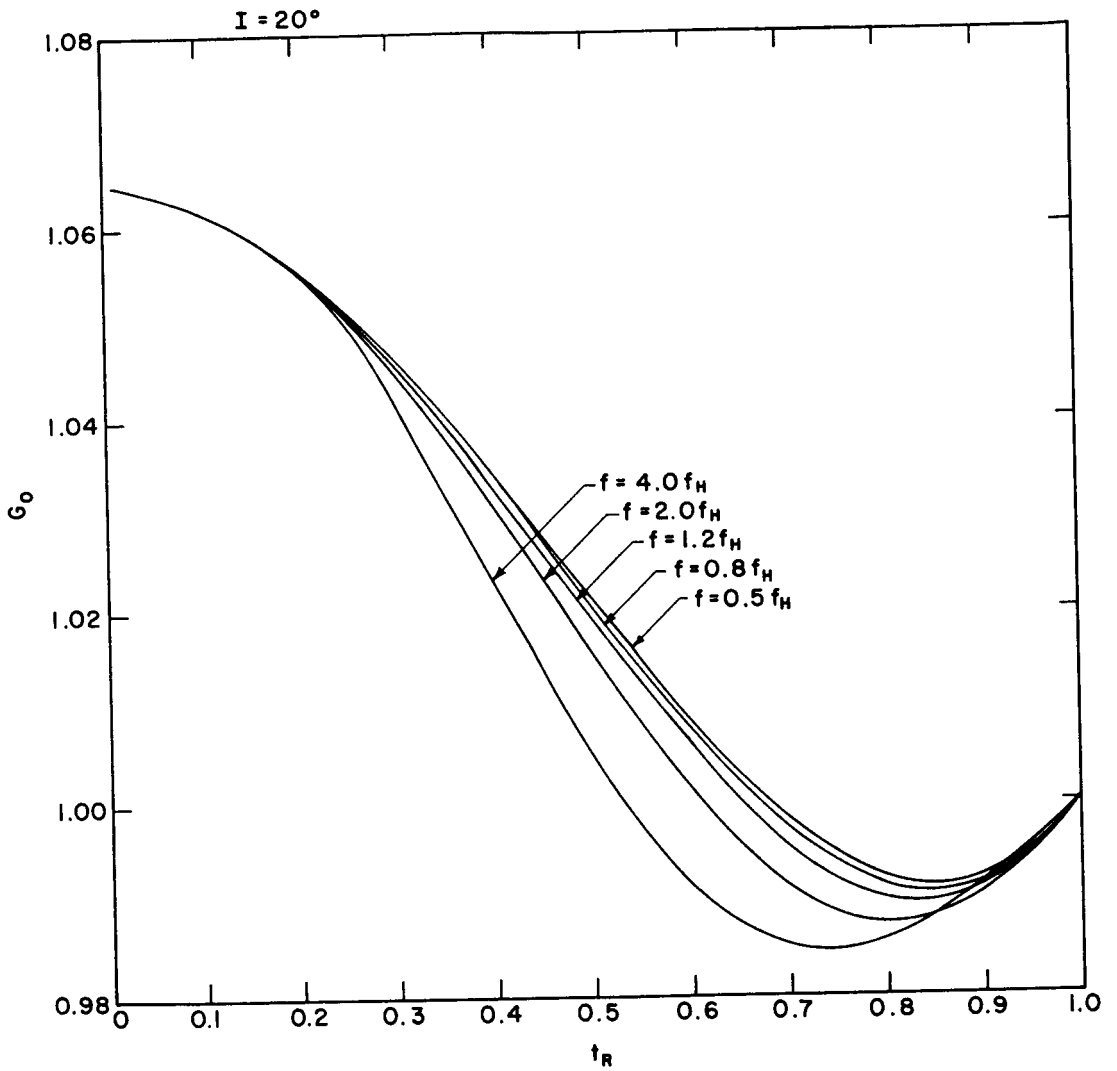
I = 20°
1.08
1.06
1.04
1.02
1.00
0.98
G_0
f = 4.0 f_H
f = 2.0 f_H
f = 1.2 f_H
f = 0.8 f_H
f = 0.5 f_H
0
0.1
0.2
0.3
0.4
0.5
0.6
0.7
0.8
0.9
1.0
t_R

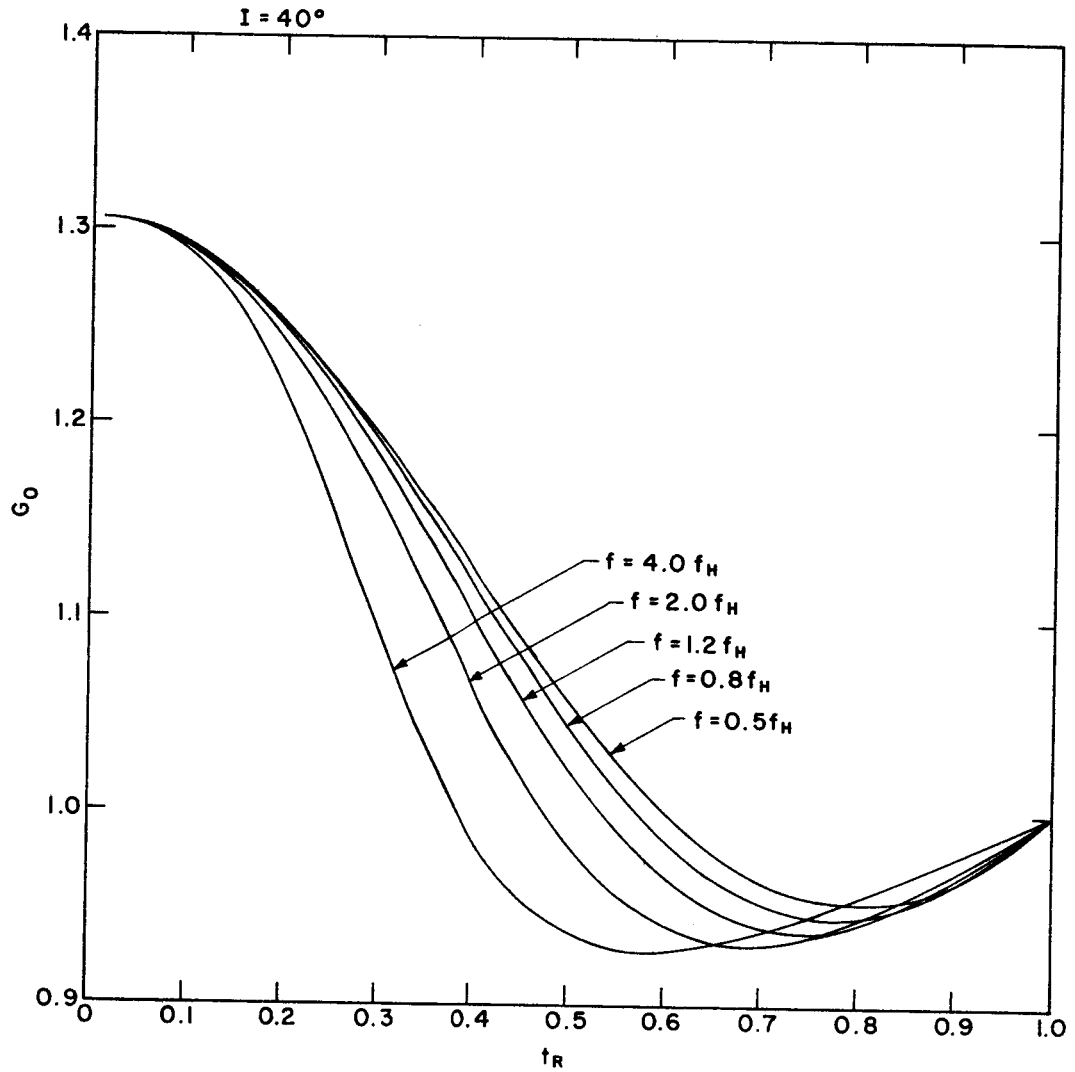
I = 40°
1.4
1.3
1.2
1.1
1.0
0.9
G_0
f = 4.0 f_H
f = 2.0 f_H
f = 1.2 f_H
f = 0.8 f_H
f = 0.5 f_H
0
0.1
0.2
0.3
0.4
0.5
0.6
0.7
0.8
0.9
1.0
t_R

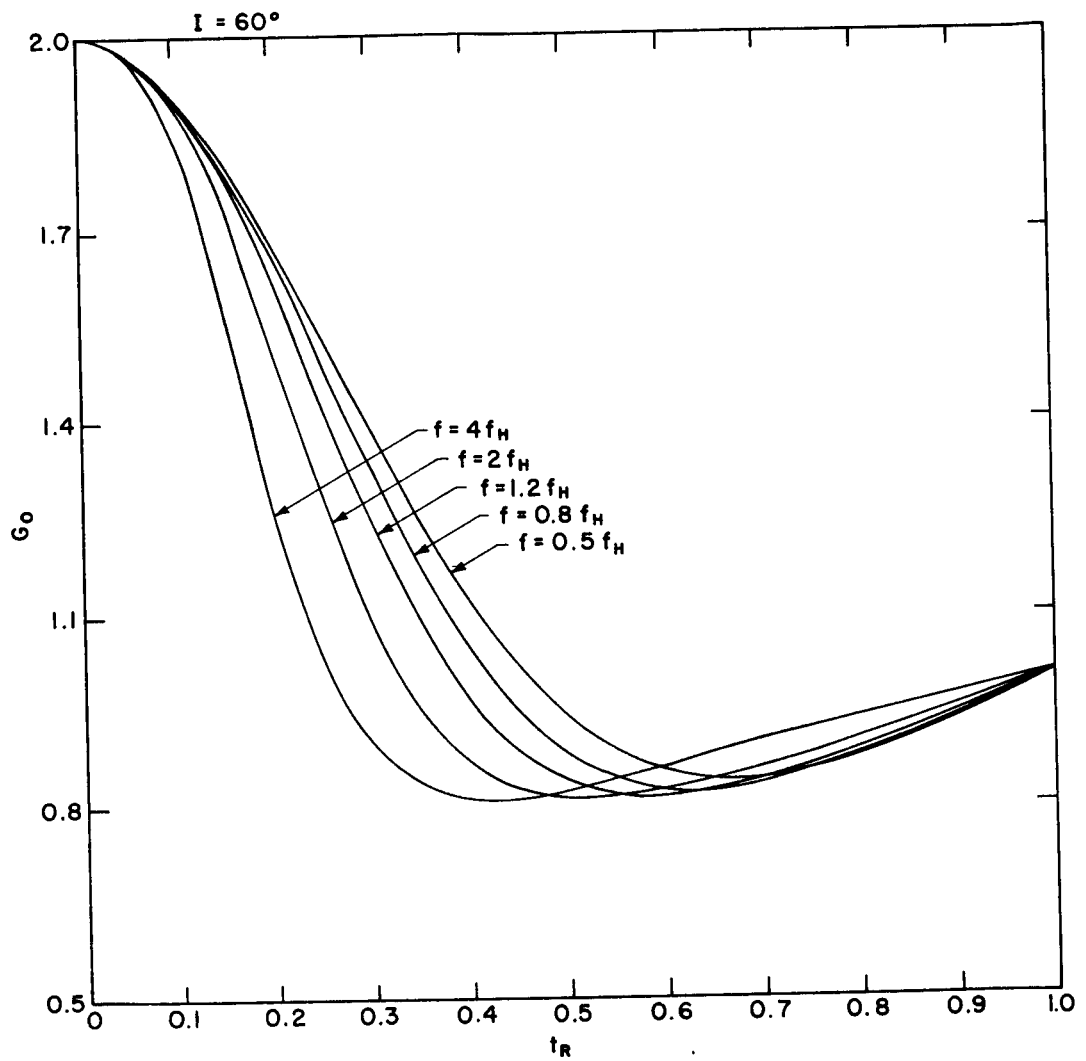
I = 60°
2.0
1.7
1.4
1.1
0.8
0.5
G_0
$f = 4f_H$
$f = 2f_H$
$f = 1.2f_H$
$f = 0.8f_H$
$f = 0.5f_H$
0
0.1
0.2
0.3
0.4
0.5
0.6
0.7
0.8
0.9
1.0
t_R

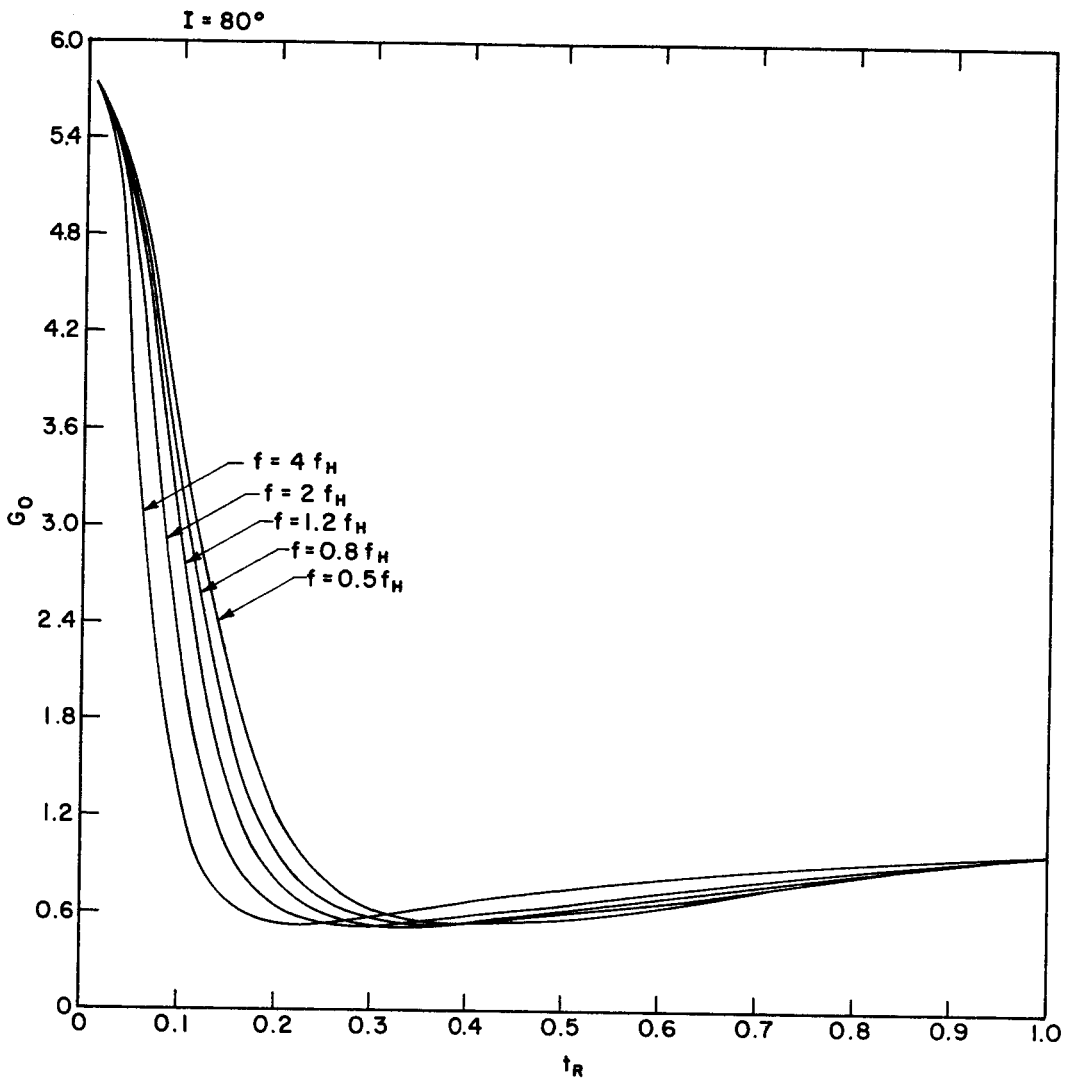
I = 80°
6.0
5.4
4.8
4.2
3.6
3.0
2.4
1.8
1.2
0.6
0
G_0
f = 4 f_H
f = 2 f_H
f = 1.2 f_H
f = 0.8 f_H
f = 0.5 f_H
0
0.1
0.2
0.3
0.4
0.5
0.6
0.7
0.8
0.9
1.0
t_R

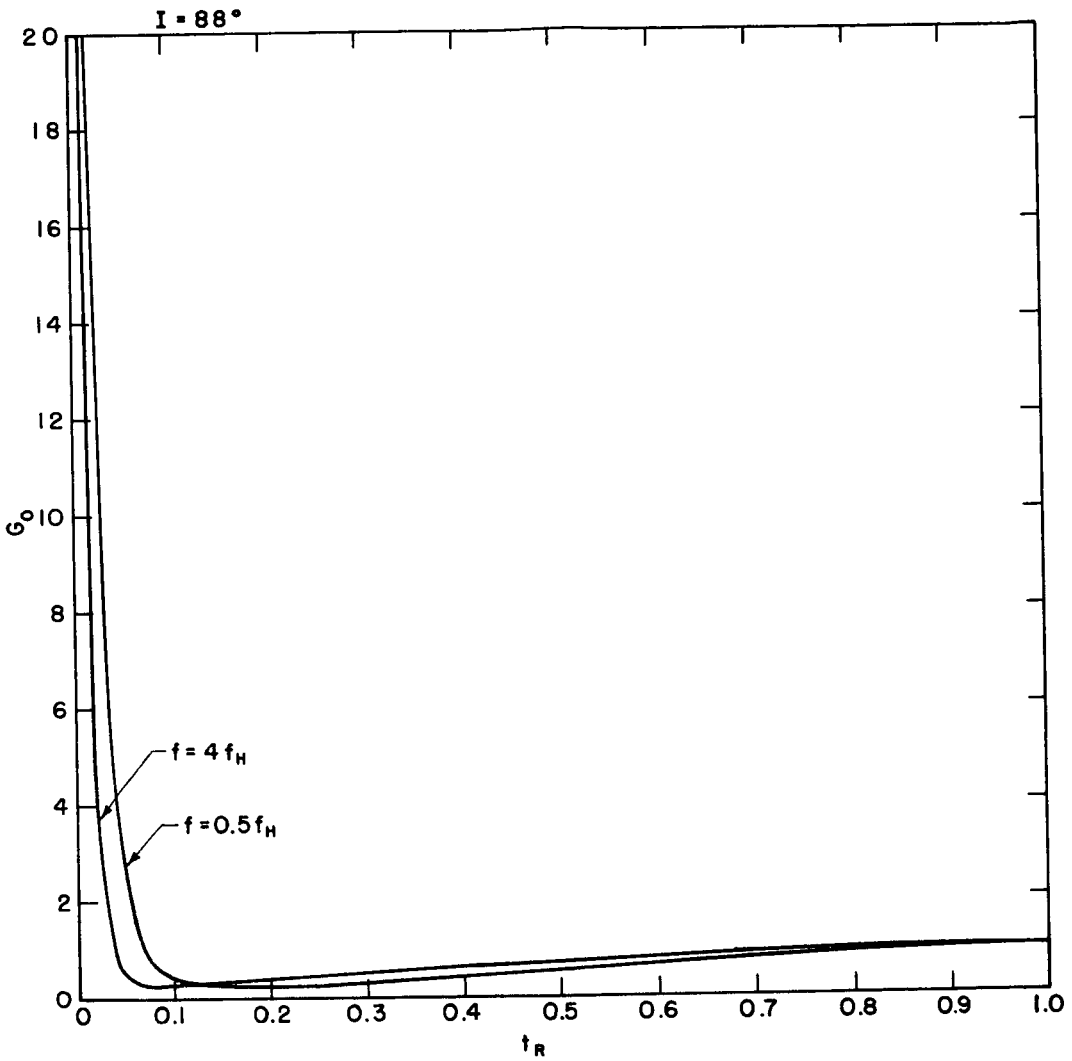
I = 88°
20
18
16
14
12
10
8
6
4
2
0
G_o
0
0.1
0.2
0.3
0.4
0.5
0.6
0.7
0.8
0.9
1.0
t_R
f = 4 f_H
f = 0.5 f_H

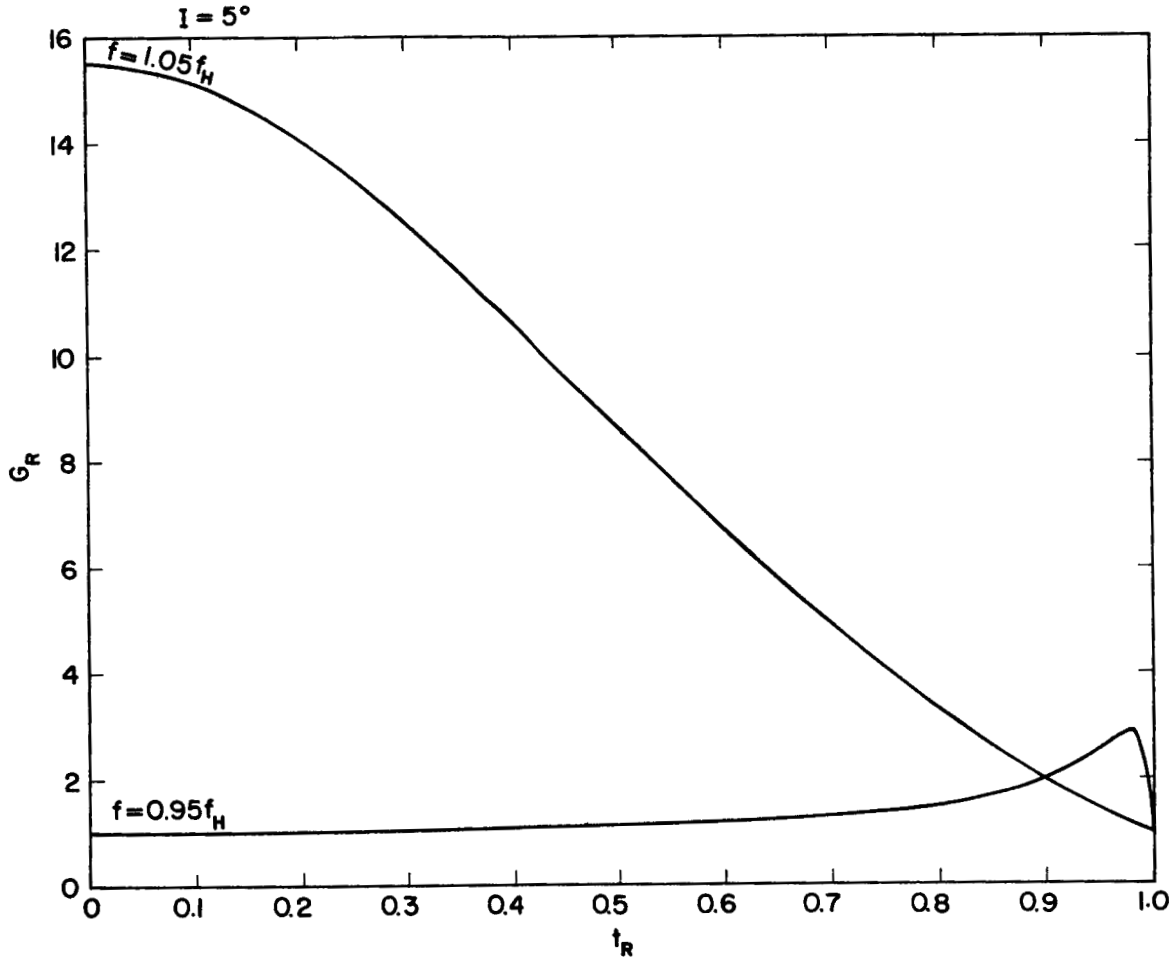

AIII.7 to AIII.18: To illustrate the behavior of the group refractive index for the Extraordinary ray. For convenience, the quantity G_R is plotted versus t_R (see text).

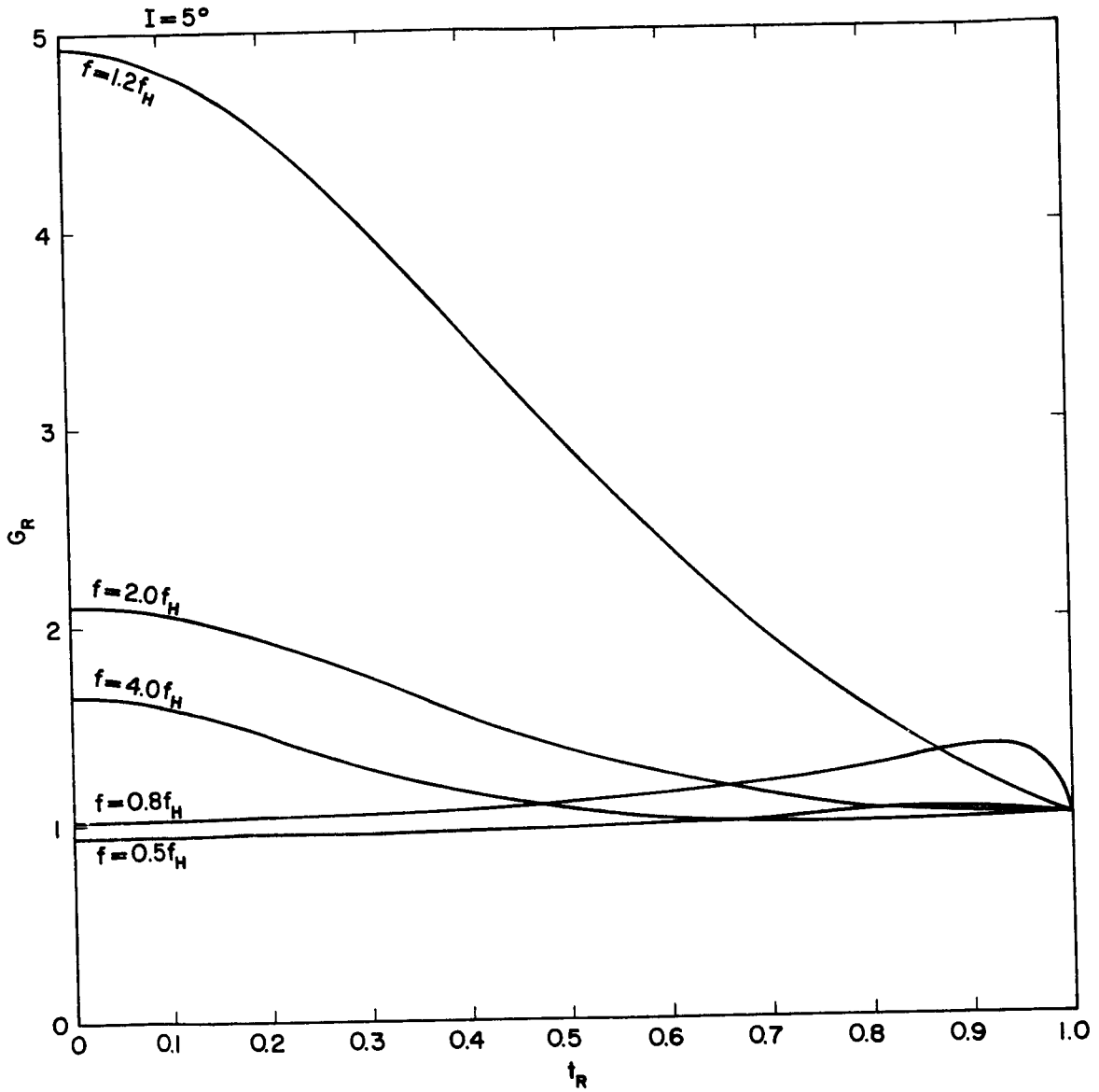
I=5°
f=1.2f_H
f=2.0f_H
f=4.0f_H
f=0.8f_H
f=0.5f_H
G_R
t_R
0
1
2
3
4
5
0
0.1
0.2
0.3
0.4
0.5
0.6
0.7
0.8
0.9
1.0

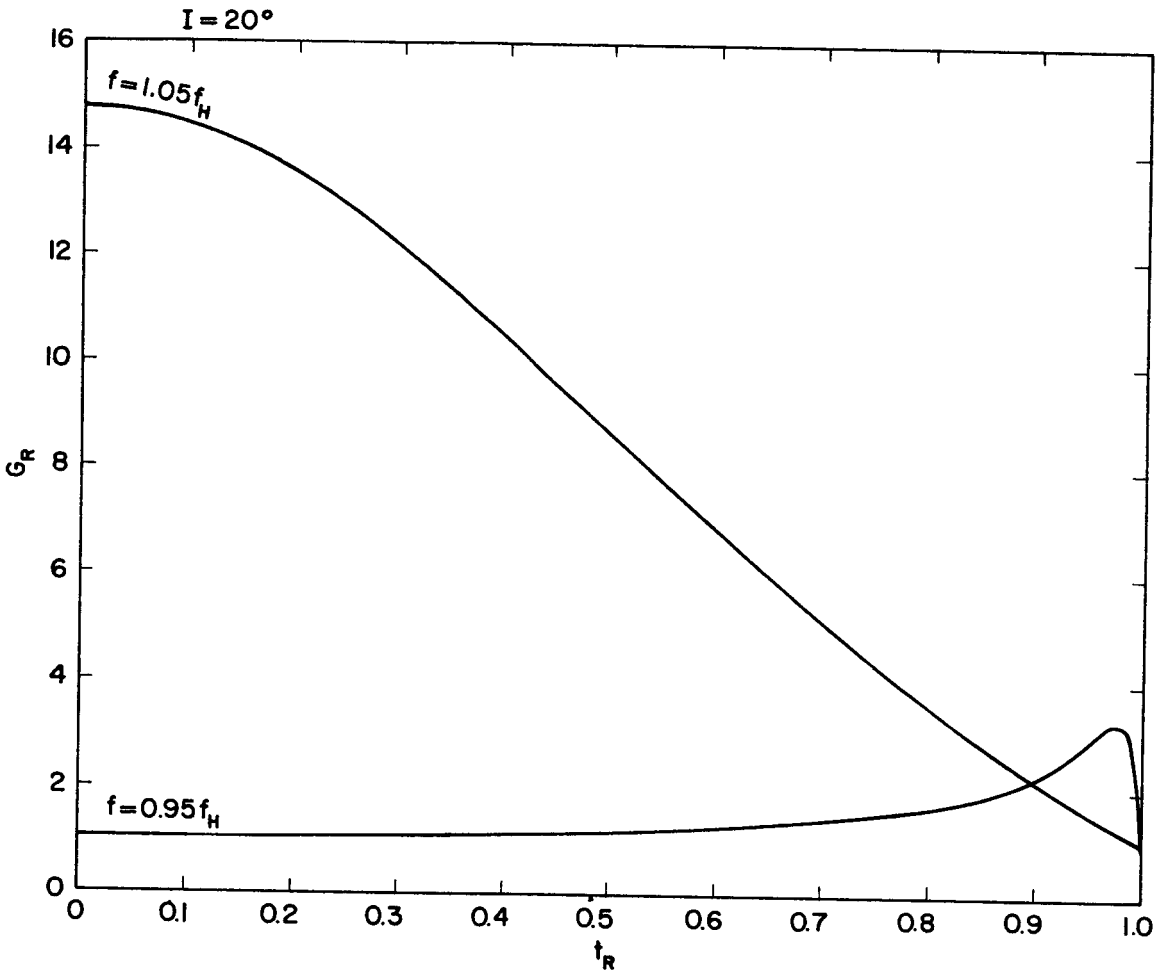
I = 20°
f = 1.05 f_H
f = 0.95 f_H
G_R
t_R
0
2
4
6
8
10
12
14
16
0
0.1
0.2
0.3
0.4
0.5
0.6
0.7
0.8
0.9
1.0

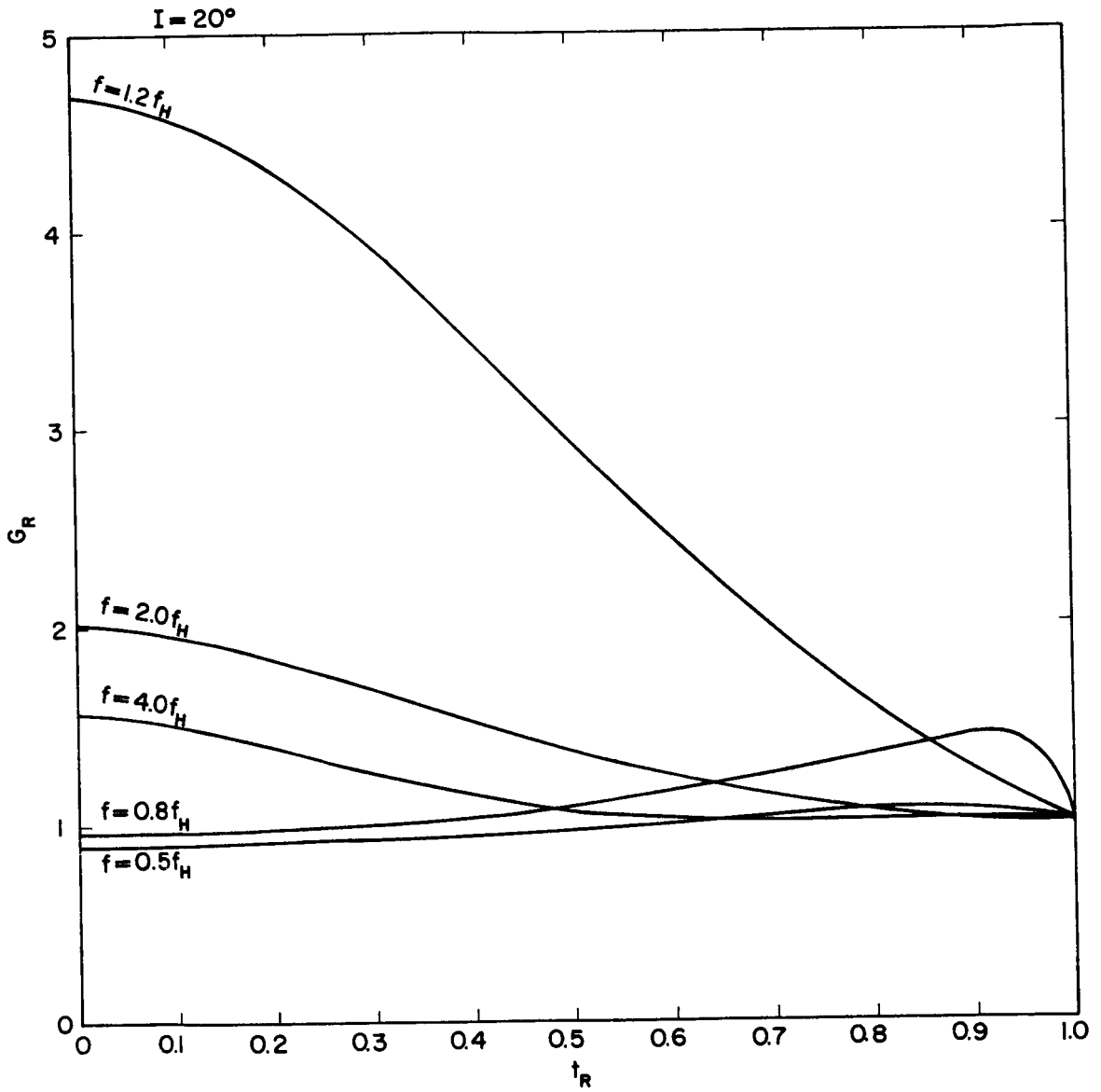
I = 20°
f = 1.2 f_H
f = 2.0 f_H
f = 4.0 f_H
f = 0.8 f_H
f = 0.5 f_H
G_R
t_R
0
1
2
3
4
5
0
0.1
0.2
0.3
0.4
0.5
0.6
0.7
0.8
0.9
1.0

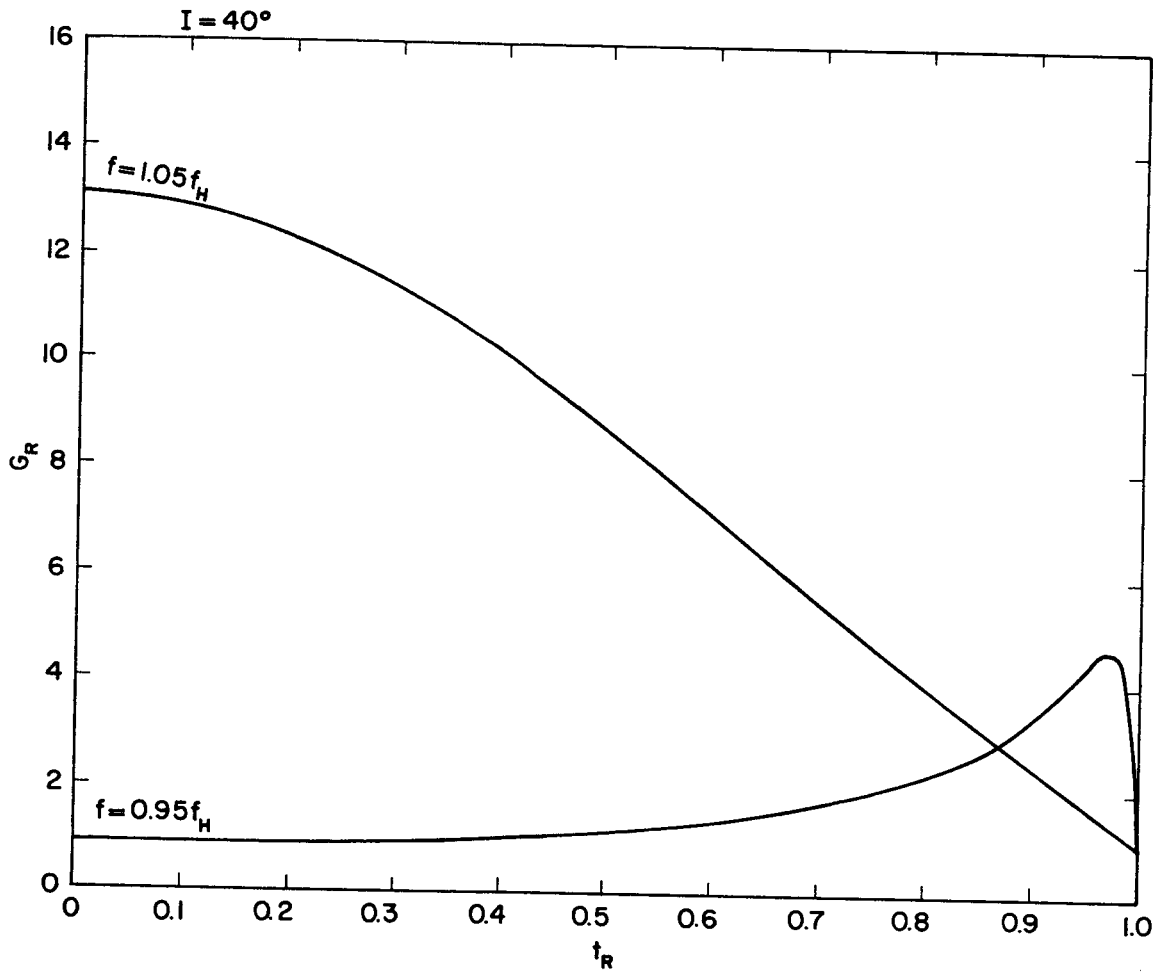
I = 40°
f = 1.05 f_H
f = 0.95 f_H
G^R
t_R
0
2
4
6
8
10
12
14
16
0.1
0.2
0.3
0.4
0.5
0.6
0.7
0.8
0.9
1.0

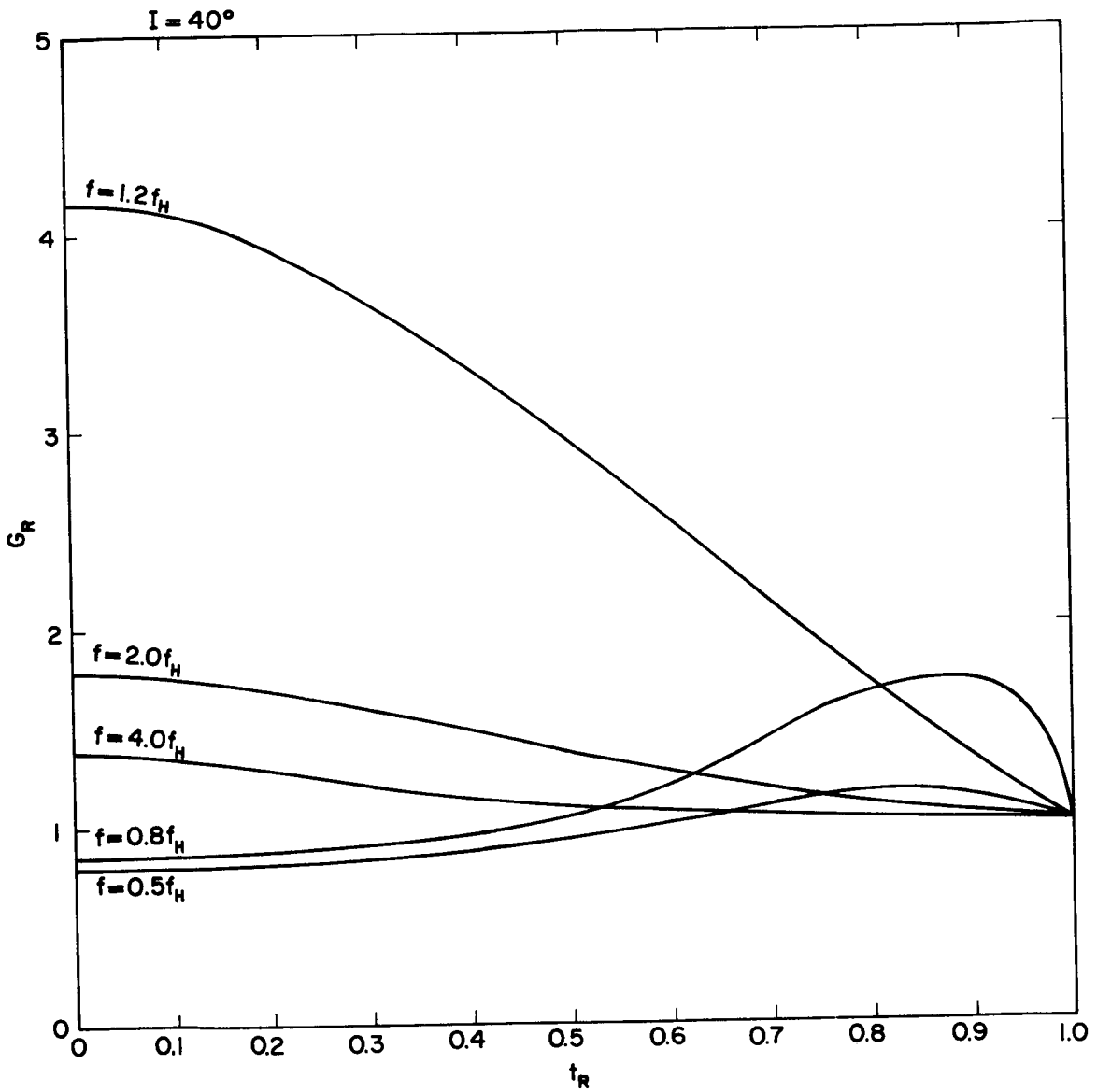
I = 40°
f = 1.2 f_H
f = 2.0 f_H
f = 4.0 f_H
f = 0.8 f_H
f = 0.5 f_H
G_R
t_R
0
1
2
3
4
5
0
0.1
0.2
0.3
0.4
0.5
0.6
0.7
0.8
0.9
1.0

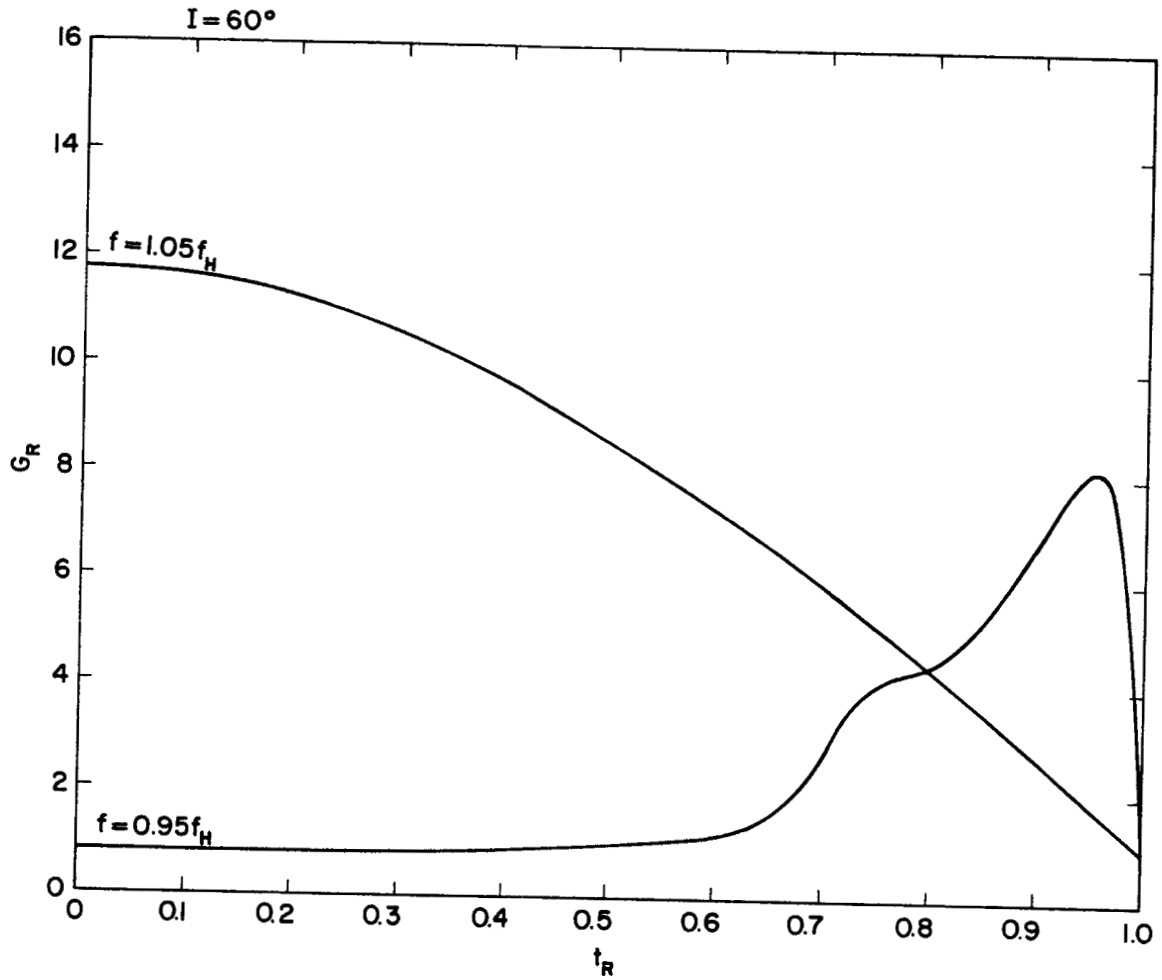
I = 60°
f = 1.05 f_H
f = 0.95 f_H
G_R
t_R
0
2
4
6
8
10
12
14
16
0.1
0.2
0.3
0.4
0.5
0.6
0.7
0.8
0.9
1.0

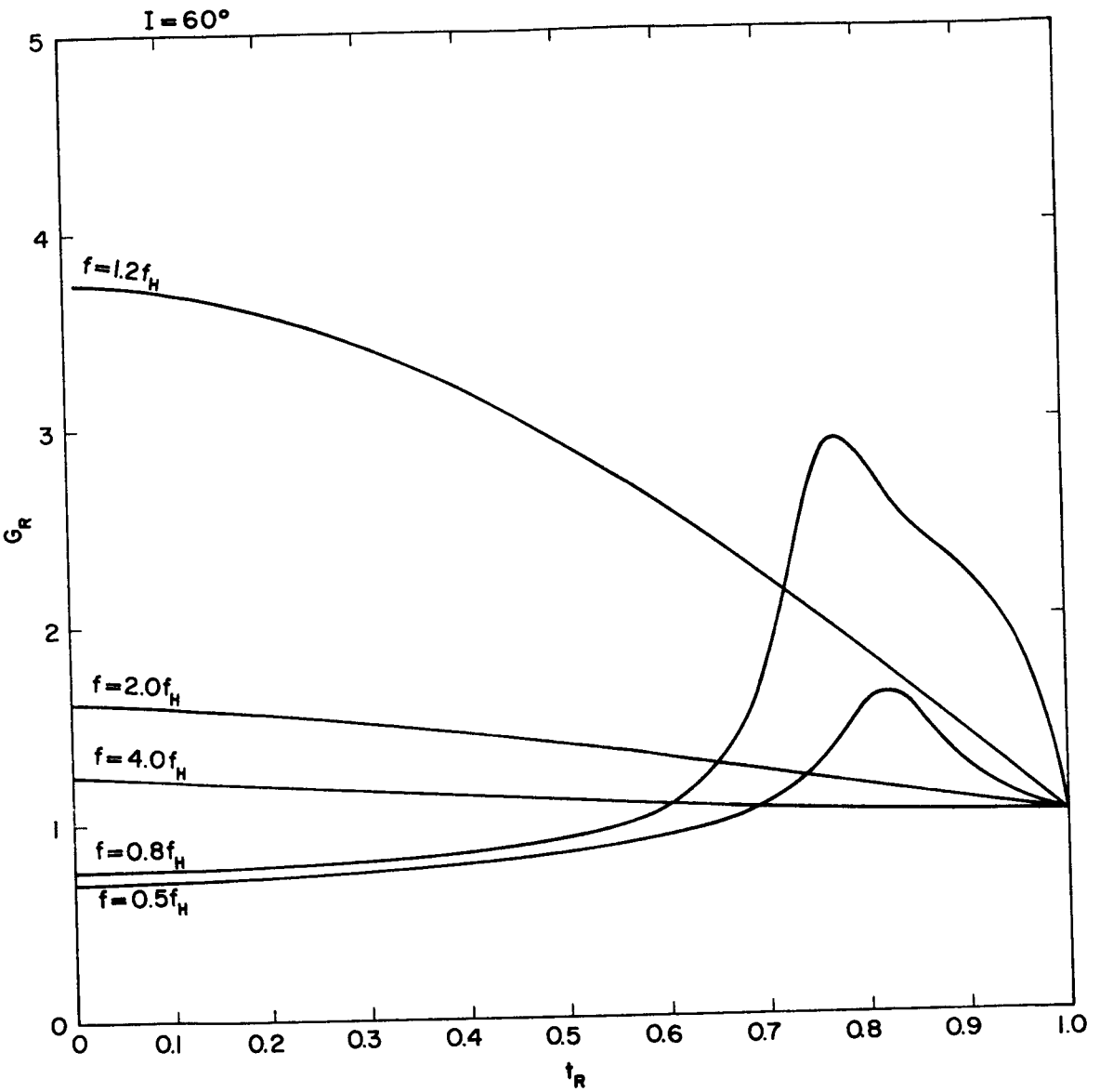
I = 60°
5
4
3
2
1
0
G_R
$f=1.2f_H$
$f=2.0f_H$
$f=4.0f_H$
$f=0.8f_H$
$f=0.5f_H$
0
0.1
0.2
0.3
0.4
0.5
0.6
0.7
0.8
0.9
1.0
t_R

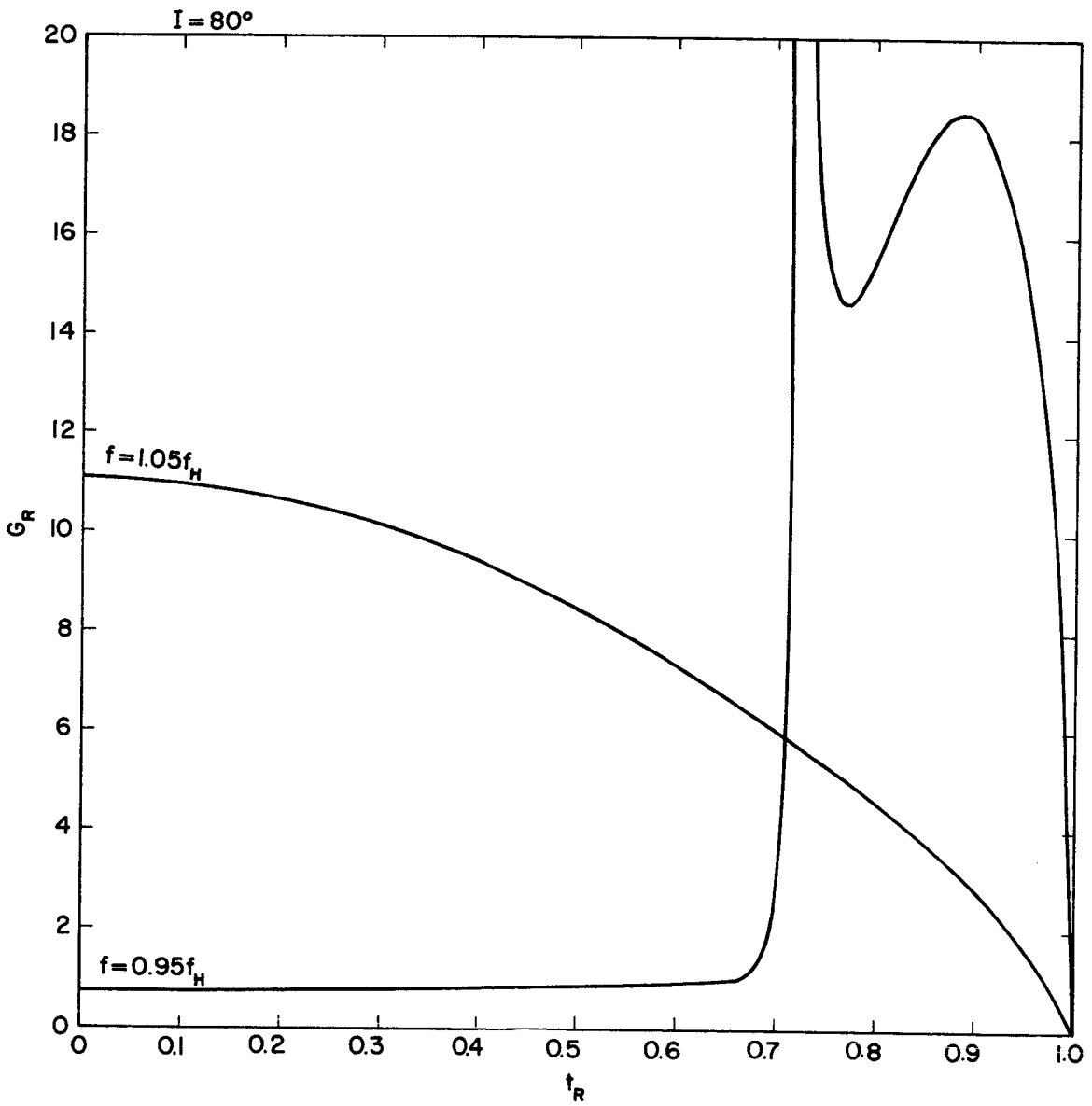
I = 80°
20
18
16
14
12
10
8
6
4
2
0
G_R
$f = 1.05 f_H$
$f = 0.95 f_H$
0
0.1
0.2
0.3
0.4
0.5
0.6
0.7
0.8
0.9
1.0
t_R

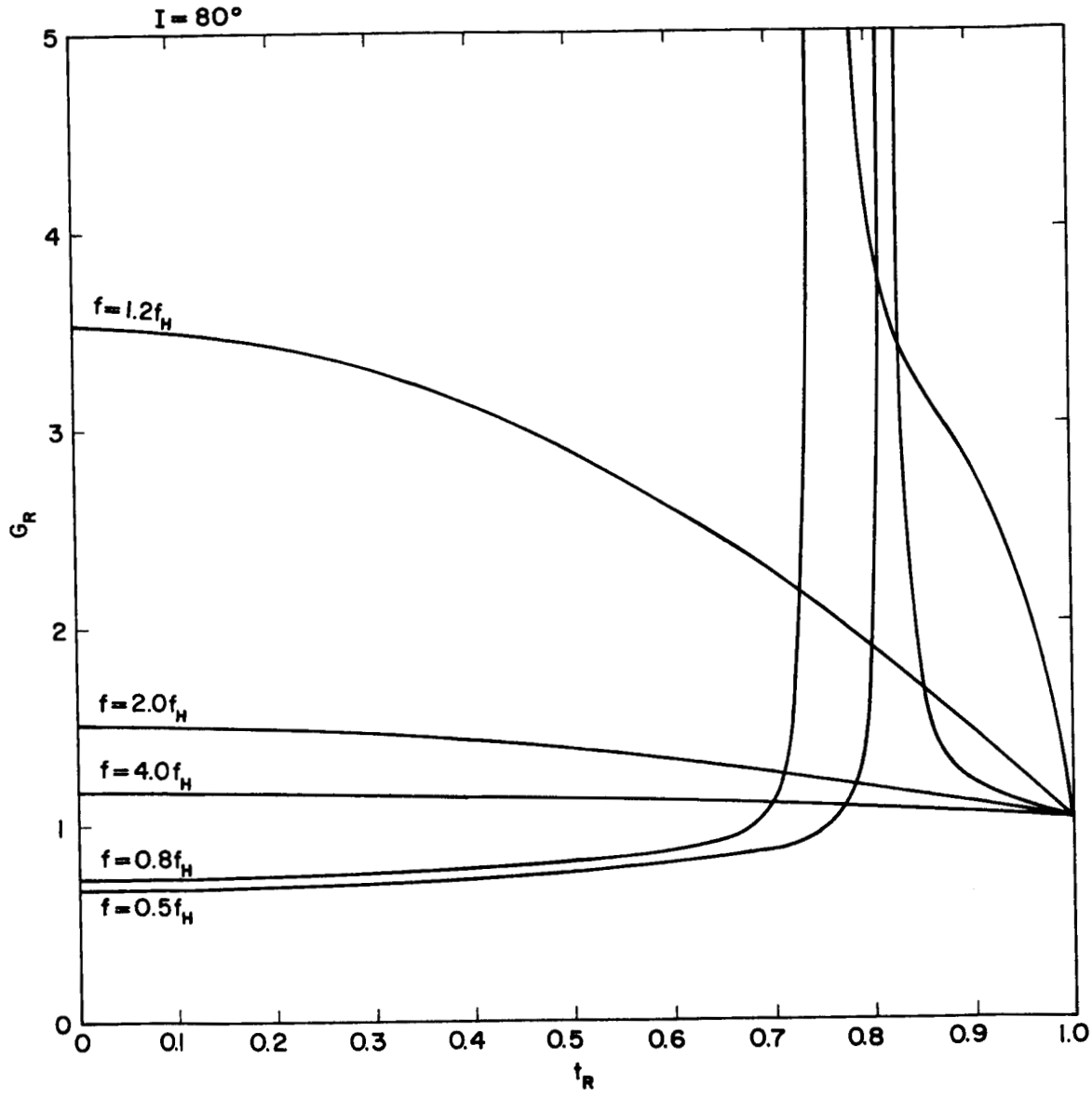
I = 80°
5
4
3
2
1
0
G_R
$f = 1.2f_H$
$f = 2.0f_H$
$f = 4.0f_H$
$f = 0.8f_H$
$f = 0.5f_H$
0
0.1
0.2
0.3
0.4
0.5
0.6
0.7
0.8
0.9
1.0
t_R

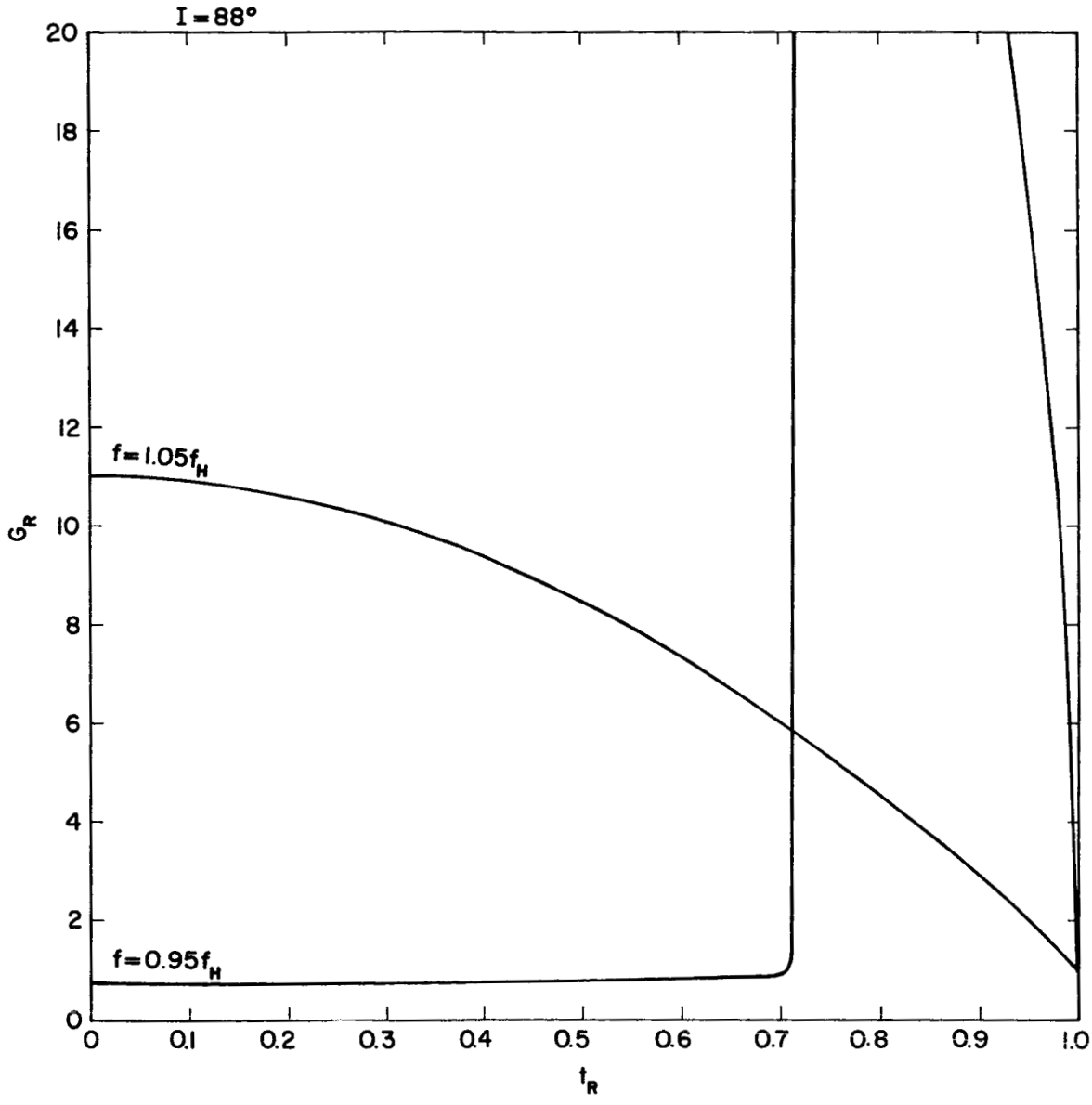
I = 88°
20
18
16
14
12
10
8
6
4
2
0
G_R
$f = 1.05 f_H$
$f = 0.95 f_H$
0
0.1
0.2
0.3
0.4
0.5
0.6
0.7
0.8
0.9
1.0
t_R

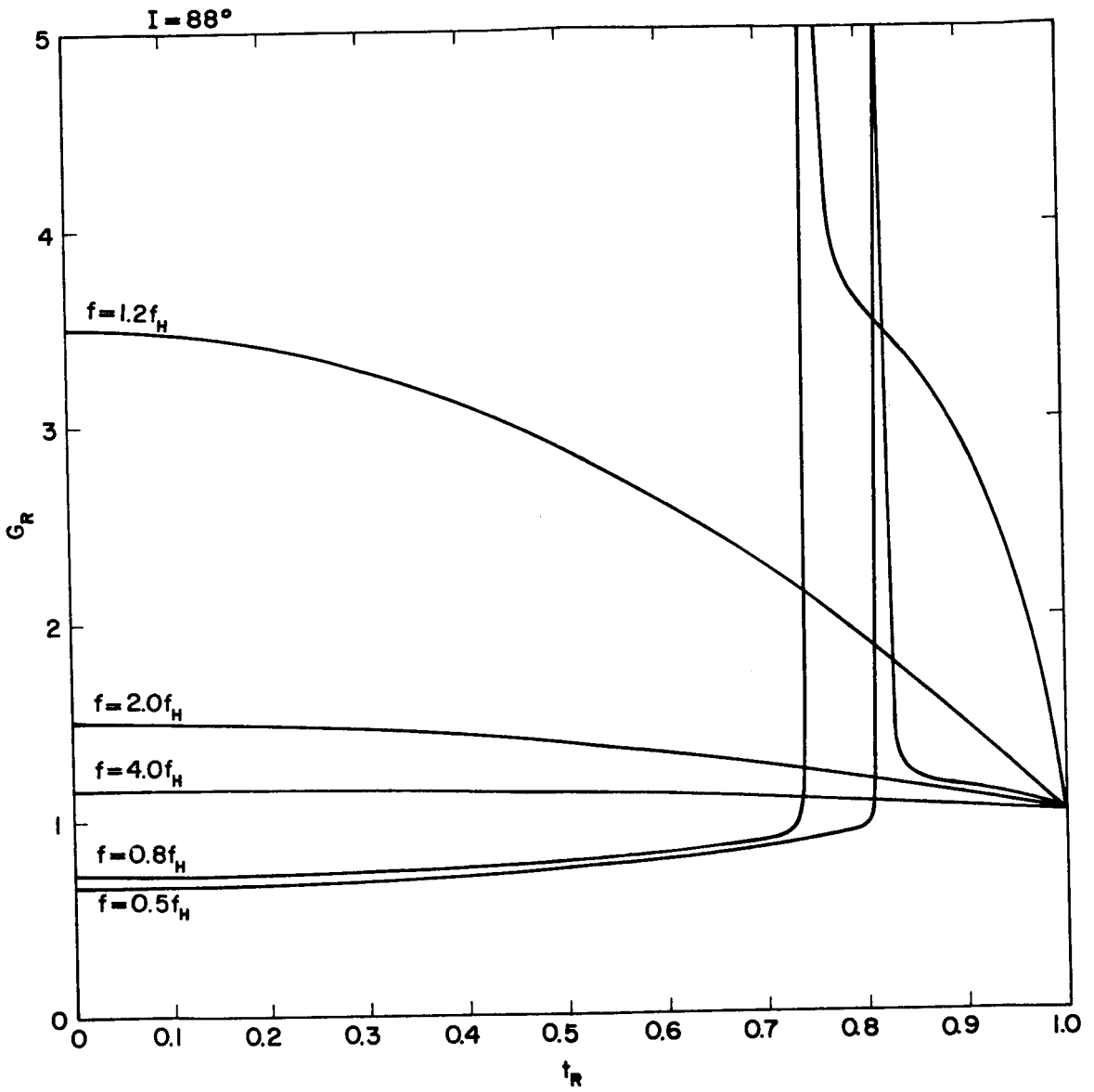
I = 88°
5
4
3
2
1
0
G_R
$f = 1.2f_H$
$f = 2.0f_H$
$f = 4.0f_H$
$f = 0.8f_H$
$f = 0.5f_H$
0
0.1
0.2
0.3
0.4
0.5
0.6
0.7
0.8
0.9
1.0
t_R

APPENDIX IV. DESCRIPTION OF COMPUTER PROGRAM

A flow chart of the computer program to carry out the calculations necessary for the reduction of virtual depth profiles to real depth profiles appears in Fig. AIV-1. In the flow chart XRAY refers to the Extraordinary ray and ØRAY refers to the Ordinary ray.

The program makes use of a number of subprograms described here to make the flow chart (Fig. AIV-1) understandable.

MUXRAY: This subroutine computes the group refractive index for the Extraordinary ray.

MUØRAY: This subroutine computes the group refractive index for the Ordinary ray.

INTEGRATE: This subroutine uses a Simpson's rule integration to evaluate the integral (see Appendix II):

$$b_{ij} = j\, f_i \int_{\sin^{-1}(f_o/f_i)}^{\pi/2} G_{o,R}(f_i \sin\theta - f_o)^{j-1}\, d\theta$$

INTEGRATE calls either MUXRAY or MUØRAY, neither of the latter two subroutines being formally called by the main program.

The Simpson's rule algorithm used in INTEGRATE provides for automatic reduction of integration variable step size, in addition to comparison of the current value of the integral with the previous value of the integral, computed with a larger step size, so that the integration may be carried out to any desired degree of accuracy.

INVERT: A matrix inversion subroutine which uses Crout's method with row interchanges. (Forsythe, 1960).

The program is written in SUBALGØL, a compiler language in use on Stanford's IBM 7090 computer. In order to allow a more universal usage of the program, a version written in FØRTRAN II is also available.

The time required to convert a 5 point virtual depth profile to a real depth profile is slightly less than 1 second.

Input and Output Data:

The program requires as input data:

1. Up to 60 characters of alpha-numeric information describing the ionogram being reduced. (e.g., pass number, date, time)

2. A digit signifying which ray, either Ordinary or Extraordinary, is to be reduced.

3. The magnetic dip angle, I, in degrees.

4. The gyro-frequency, f_{Hv}(Mc/s) at the location of the satellite. This quantity is computed for each record in a separate program (Thomas and Sader 1963).

5. The number of sample frequencies and corresponding virtual depths.

6. The plasma frequency at the satellite. For the Ordinary ray, f_o is used; for the Extraordinary ray, f_{xv} is used.

7. The sample frequencies and corresponding virtual depths. For the Ordinary ray, f_i is used; for the Extraordinary ray, f_{xi} is used.

Output from the program consists of:

1. Ionogram identification as specified on the input.

2. The gyro-frequency, f_{Hv}, at the location of the satellite.

3. The plasma frequency, f_o, at the satellite. If the Extraordinary ray is used, this is calculated from f_{xv} and f_{Hv} by Eq. (10).

4. For the Ordinary ray: The Ordinary ray sample frequencies (plasma frequencies) with the corresponding virtual depths and real depths.

5. For the Extraordinary ray: The Extraordinary ray sample frequencies with the corresponding virtual depths, the plasma frequencies, corresponding to the sample frequencies, and the corresponding real depths.

In the case of the Extraordinary ray, the plasma frequencies are the "modified" plasma frequencies, obtained by the technique described in Appendix VI.

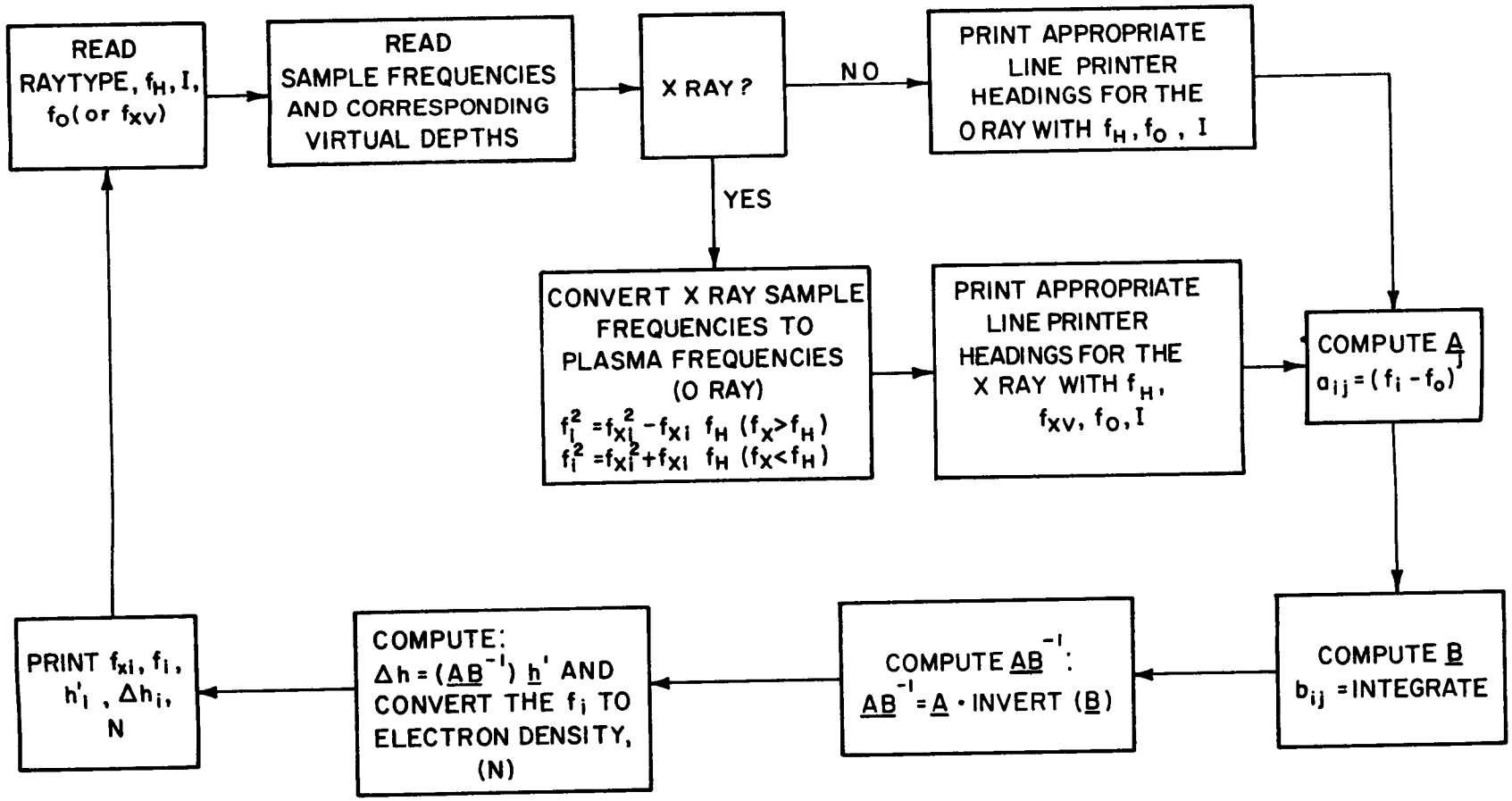

AIV.1: Flow diagram to illustrate the arrangement of the h'(f)-N(h) calculation in the digital computer program.

APPENDIX V. TECHNIQUES USED TO SYNTHESIZE THEORETICAL $h'_x(f)$ CURVES FOR AN EXPONENTIAL LAYER

Figures 11 and 12 in the main text represent the $h'_x(f)$ virtual depth profiles one would expect to observe assuming an exponential real depth profile of the form:

$$f_o^2 = f_v^2 \, e^{(h_o - h)/H} = f_v^2 \, e^{\Delta h/H} \qquad \text{(AV-1)}$$

where f_o is the plasma frequency and f_v is now written for the value of f_o at the vehicle.
The Extraordinary virtual depth is:

$$h'_x(f) = \int_{\Delta h=o}^{\Delta h=h_R} \frac{c}{U_x} \, d(\Delta h) \qquad \text{(AV-2)}$$

where h_R is the real depth of reflection, that is, the depth at which

$$\frac{f_o^2}{f_R^2} = 1 \text{ or } t_R = o \qquad \text{(AV-3)}$$

As before:

$$x_R = \frac{f_o^2}{f_R^2}$$

$$t_R^2 = 1 - x_R \qquad \text{(AV-4)}$$

Equation (AV-2) then becomes, writing $a = (1 - f_v^2/f_R^2)^{\frac{1}{2}}$

$$h'_x(f) = 2\int_{t_R=o}^{t_R=a} \left(\frac{c \cdot t_R}{U_x}\right) \frac{d(\Delta h)}{dx_R} \, dt_R \qquad \text{(AV-5)}$$

or:

$$h'_x(f) = 2\int_{t_R=o}^{t_R=a} G_R \cdot \frac{d(\Delta h)}{dx_R} \, dt_R \qquad \text{(AV-6)}$$

The expression in (AV-1) may be rewritten as:

$$\left.\begin{aligned} \frac{f_o^2}{f_R^2} = x_R &= \left(\frac{f_v}{f_R}\right)^2 e^{(h_o-h)/H} \\ \text{or} \qquad \Delta h &= H \log x_R - H \log\left(\frac{f_v}{f_R}\right)^2 \end{aligned}\right\} \quad \text{(AV-7)}$$

and

$$\frac{d(\Delta h)}{dx_R} = \frac{H}{x_R} \qquad \text{(AV-8)}$$

Combining this expression with (AV-6), the expression for the exponential layer Extraordinary virtual depth curve becomes:

$$h'_x(f) = 2H\int_{t_R=o}^{t_R=a} \frac{G_R}{x_R}\, dt_R \qquad \text{(AV-9)}$$

APPENDIX VI. EFFECT OF VARYING MAGNETIC CONDITIONS

Figure AVI·1 shows the variation of the gyro-frequency, f_H, with height from ground-level to 2000 km assuming an inverse cube-law variation. It is clear from this that the gyro-frequency may vary over the path which a radio wave traverses from the satellite to reflection point by as much as 0.5 Mc/s when the satellite is, say, at 1400 km and the reflection point near the peak of the F2 layer. For accurate work, this variation would have to be allowed for in computing the matrix elements in C.

The quantity f_H enters the computation via the expressions for μ_o' and μ_x'. More importantly, the value of f_H affects the limits in Eq. (11) and it is therefore extremely important to allow for the variation of f_H with height for the case of the Extraordinary ray. Unfortunately, in practice, this cannot be done directly since the height h corresponding to a particular value of the plasma frequency is in fact the unknown in the calculation so that the appropriate value of f_H cannot be determined. It appears adequate, however, to read into the machine the value of f_H at the vehicle and to calculate the N(h) profile using this parameter. The plasma frequency at a given height is then corrected using the relationship

$$f_{xi}^2 = f_i'^2 + f_{xi} f_{Hi}$$

where the f_H used in this formula corresponds to the f_H at the calculated real depth, assuming an inverse cube variation of f_H from the value at the vehicle to that at the real depth in question. This technique was suggested by Doupnik (1963).

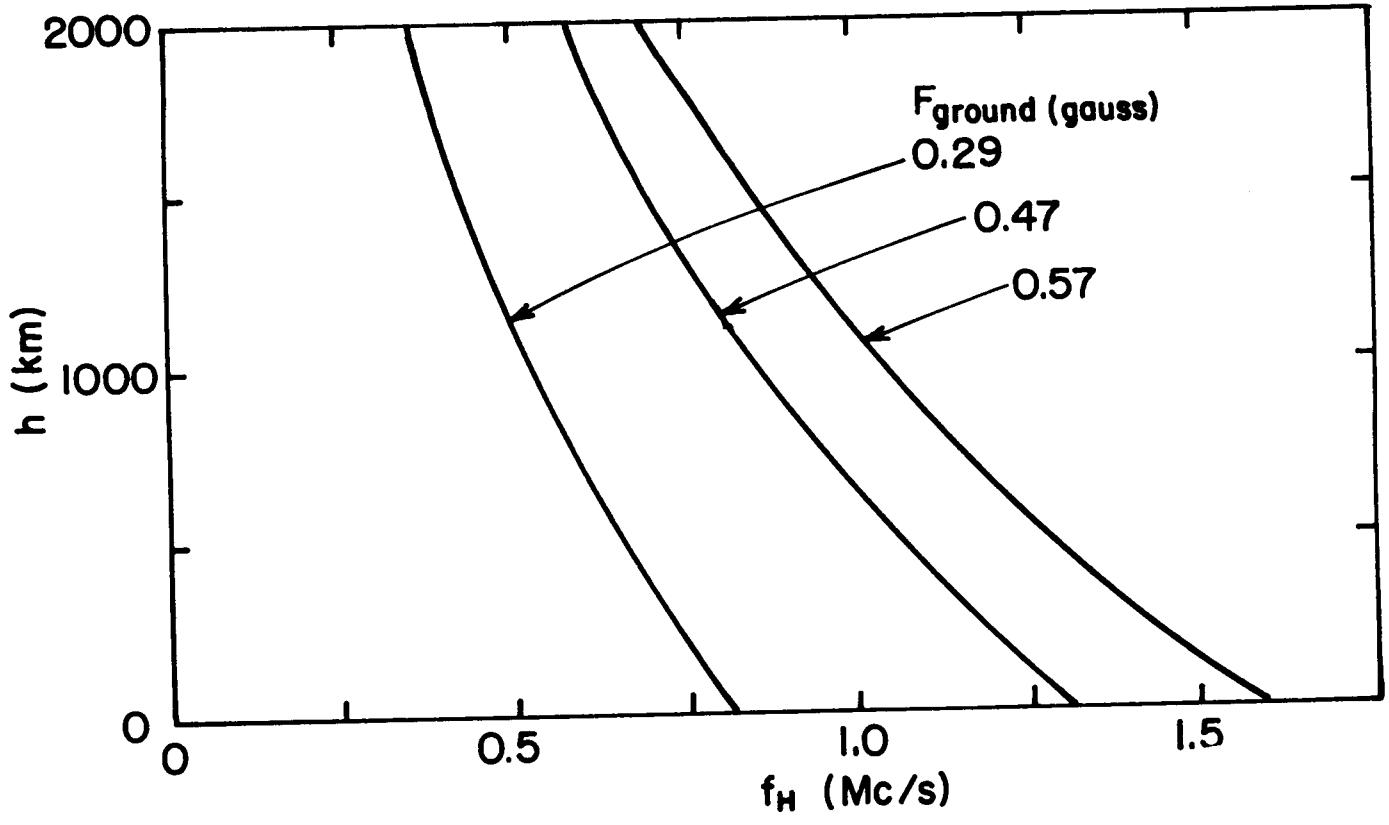

AVI.1: Variation of gyrofrequency f_H with height for different values of the earth's total field F at the ground.

REFERENCES

Becker, W., "Das Vergleichsverfahren der Station Lindau/Harz zur Bestimmung der wahren Verteilung der Elektronendichte in der Ionosphare," A.E.U., 13, 49, 1959

Becker, W., "Tables of Ordinary and Extraordinary Refractive Indices, Group Refractive Indices and $h'_{o,x}(f)$ Curves for Standard Ionospheric Layer Models, Max-Plank Institute for Aeronomy, 4, 1960

Becker, W., Private Communication, 1963

Budden, K.G., "Radio Waves in the Ionosphere," Cambridge University Press, 151, 1961

C.D.R.T.E., Alouette, Satellite 1962 Beta Alpha One, published by the Canadian Defence Research Board, Ottawa, 1962

Doupnik, J.R., "A Flexible Method of Determining the Electron Density Distribution in the Ionosphere," Scientific Report No. 190, Ionosphere Research Laboratory, Pennsylvania State University, 1963.

Forsythe, G.E., Algorithm 16, Crout with Pivoting, "Communications of the Association for Computing Machinery," 507, 1960

Knecht, R.W., van Zandt, E., & Watts, J.M., The NASA fixed frequency topside sounder program. Paper in "Electron Density Profiles in the Ionosphere & Exosphere," edited by B. Maehlum, Pergamon Press, 246, 1962

Lockwood, G.E., Plasma and cyclotron spike phenomena observed in topside ionograms. Paper presented at URSI-IRE meeting, Ottawa, October 1962

Long, A.R., & Thomas, J.O., Titheridge coefficients for the polynomial method of deducing electron profiles from ionograms, J. Res. Nat. Bur. Standards - D. Rad. Prop., 67D No. 1, 79, 1963

Shinn, D.H., Tables of group refractive index for the ordinary ray in the ionosphere, "The Physics of the Ionosphere," Proc. Cambridge Ionosphere Conference, Physical Society, London, 402, 1954

Thomas, J.O., Long, A.R., & Westover, D., "The Calculation of Electron Density Profiles from Topside Sounder Records," J. Geophys. Res., 68, No. 10, 3237, 1963

Thomas, J.O., & Sader, A., A report on Alouette Topside Soundings monitored at Stanford University, TR No.6, Stanford Electronics Laboratories (in press) 1963

REFERENCES (Continued)

Thomas, J.O., & Westover, D., to be published (1963)

Thomas, J.O., & Vickers, M.D., The conversion of ionospheric virtual height-frequency curves to electron density-height profiles. DSIR Radio Research Special Report No. 28. Her Majesty's Stationery Office, London, 1959.

Thomas, J.O., The Canadian Topside Sounder "Alouette," Science, 139, 229, 1963

Titheridge, J.E., A new method for the analysis of ionospheric h'(f) records, J. Atmos. Terr. Phys., 21, 1, 1961.

van Zandt, T.E., Private communication 1961.

Warren, E.S., "Sweep Frequency Radio Soundings of the Topside of the Ionosphere," Can. J. Phys., 40, 1692, 1962